12-15-2016

Comprehensive Applications of Rice Husk Biomass

Zichao Wei
University of Connecticut,Storrs, zichao.wei@uconn.edu

Comprehensive Applications of Rice Husk Biomass

Zichao Wei

B.E., Shenyang University of Chemical Technology, 2014

A Thesis

Submitted in Partial Fulfillment of the

Requirements for the Degree of

Master of Science

At the

University of Connecticut

2016

2016

APPROVAL PAGE

Master of Science Thesis

Comprehensive Applications of Rice Husk Biomass

Presented by

Zichao Wei, B.E.

Major Advisor_____
Dr. Luyi Sun

Associate Advisor_____
Dr. Richard Parnas

Associate Advisor_____
Dr. Jie He

University of Connecticut

2016

Acknowledgements

I would like to thank my major advisor Dr. Luyi Sun for his guidance and support through my whole master degree's study. I appreciate his patient, comments, contribution of time and precisely academic attitude. His encouragement and advices are the cornerstones to make me complete this decent work. He also provided many advices, suggestions and experience for my career and personal life to give me enormous help. I am honored to have such a good and wisdom mentor.

I also want to express my gratitude to my committee members, Dr. Richard Parnas and Dr. Jie He for their valuable time, supports and precious comments for my master thesis and defense.

I'm grateful to Dr. Zhaofeng Wang, the former postdoctoral lab mates for his guidance on my research experience. He is a good teacher and helpful friend. I also would like to thank all the group members and all my friends in University of Connecticut. It's my pleasure and glad to meet with you. At the same time, I specially want to thank the undergraduate students, Mr. William R. Tait and Ms. Alice Hu for their assistance on my research and defense.

Mostly, I would like to thank my parents, Zeguo Wei and Xiaochun Jiang for their endless love, encouragement and support.

Table of Contents

List of Figures

List of Tables

Comprehensive Applications of Rice Husk Biomass

Zichao Wei, M.S.

University of Connecticut, 2016

Rice husks (RHs) have recently attracted high attention due to their potential for many applications, including construction materials, composite materials, adsorption materials, chemical production, and power generation. RHs are an appealing alternative because of their low cost and high silica content. So far, most researchers mainly focus on the utilization of one component (such as silica) while ignoring others. Comprehensive utilization of RH biomass and diversified products are the key goals for this research field.

In this thesis, the two main components of RHs, silica and lignocellulose, were extracted from RH biomass. The high tempered calcination served as the extraction process of the highly reactive RH silica nanoparticles. Because of its remarkable physiochemical properties, green phosphor of Zn_2SiO_4:Mn^{2+} was synthesized under a high temperature pyrolysis method. This study also investigated the effects of reaction temperature and Mn^{2+} doping concentration on the photoluminescence properties of the RH silica phosphor. By comparing with the phosphor prepared from commercially used silica, RH silica phosphor showed superior photoluminescence properties. Because RHs are an inexpensive resource and the RH silica phosphor exhibited better performance, it should be considered a promising alternative.

The second part of the thesis studied the extraction of the lignocellulose from RH biomass by using ionic liquid (BMIMCl). Through liquid nitrogen frozen and thaw (NFT) process, water regeneration, and CO_2 supercritical drying, the light and porous lignocellulose aerogel was prepared. In addition, the lignocellulose aerogel can be further converted to a carbon aerogel via a facile pyrolysis process. Because of the inherited porous structure, the carbon aerogel is expected

to find wide applications in many areas. Silane agent (MTMS) modification of the lignocellulose aerogel is another route to expand its applications. The treated lignocellulose aerogel exhibited to be highly hydrophobic, making it effective in oil spill adsorption. Based on the comprehensive utilization strategy, the RH residue separated from IL solution was used to prepare highly active and amorphous silica nanoparticles, which also have widespread application.

Chapter 1. Introduction: Comprehensive Applications of Rice Husks

1.1 Introduction

Rice is one of the most common food crops in the world. Additionally, it is one of the largest sources of biomass, namely, rice husks (RHs). In the past, RHs were considered as a waste. Farmers disposed of RHs by open-field burning, which generated significant pollution, especially in developing countries [1]. Researchers have found that RHs contain silica (15-28 wt. %) and lignocellulose (LC, 72-85 wt. %), which can be further categorized into cellulose (35-40 wt. %), hemicellulose (15-20 wt. %), and lignin (20-25 wt. %). The exact weight percentages of these components are determined by the water quality, environment, climate, and soil conditions of where the rice is grown [2]. Because of the high concentration of lignocellulose and silica in RHs, RH biomass can be applied for a wide variety of areas, including chemical production, construction materials, agriculture, adsorption materials, and power generation. In these applications, RH biomass exhibits two major advantages: low cost and sufficiently good quality. Considering RHs contains both inorganic silica and organic lignocellulose, it is highly desirable to derive both components for practical applications. In this way, RHs can serve as a sustainable and cost-effective resource for various industries.

1.2 Chemical Production

Lignocellulose and silica are the main contents in RHs. They can be used as alternative resources in the production of chemical products, such as active carbon (AC), fibers, and syngas. RHs can also be used in the production of biofuel. The low price and massive quantity of RHs make them an attractive resource compared to other biomasses.

1.2.1 Active carbon

Active carbon (AC) is a known adsorbent that exhibits a high adsorption capacity and large surface area [3]. It has been widely used as a catalyst support [4], gas storage material [5] and adsorbent material [6]. Many biomasses can serve as the precursor of AC, including sunflower shells [7], corn straws [8], olive stones [9], cotton residues [7], etc. RHs biomass can also play an important role in AC production because of its high organic content and low price. The physical activation method and chemical activation method can be used to transfer RH biomass to AC.

For the physical method, the carbonization process will be completed under nitrogen or inert gas atmosphere at a temperature range of 600-900 ℃. Activation will occur at high temperatures, 600-1000 ℃, when the sample is exposed to an atmosphere of steam, carbon dioxide, or the combination of the two gases. For the chemical method, impregnation of RHs is assisted by alkaline, alkali carbonates, acids, or metal salts. Then the sample is activated with N_2 at temperature of 400-900 ℃.

Applications of AC are widespread. Zhu et al. [10] explored the physical activation method to make AC from RHs. Their results showed that the prepared AC can effectively remove NH_4^+ ions, and there was an increased ion removal with an increased dosage. Yao et al. [11] recently used microwave-assisted nitric acid oxidation to modify the AC from RHs. They found that the modified AC exhibited a fast adsorption of Pb (II) than the un-modified one. Mashhadi et al. [12] used a similar modification method by using sulfuric acid to make AC for the removal of Hg (II). Besides as an adsorbent, RH derived AC could also be applied for catalyst support [13] and hydrogen storage [14] because of its high meso-porosity and surface area.

1.2.2 Fibers

Because of the high content of lignocellulose (including cellulose, hemicellulose and lignin), RHs can be used to prepare natural fibers. Natural cellulose fibers can be extracted from lignocellulose by using bacterial, fungal, mechanical, or chemical methods [15]. Cellulose fibers from RHs could be extracted by bacteria and fungi, an environmentally friendly and energy-saving process yet time-consuming. The more common process of extraction is the chemical method. Sodium hydroxide, sulfuric acid, and oxalic acid are the typical chemicals used to remove the components other than cellulose from RHs. As shown in Figure 1a and 1b, the alkali treatment made the smooth surface of RH fibers rougher, which suggests that alkali could remove some impurities from the cellulose components. Figure 1c shows that the acetic bleaching process separated RH fiber bundles into individual fibers. Figure 1d shows that the acid hydrolysis treatment cleaved the amorphous region of cellulosic micro-fibrils transversely, keeping the straight crystalline domains intact. This allows the cellulose derived from RHs to be used as a nanomaterial, which could be applied for advanced applications, such as photonic crystalline materials [16], graphene quantum dots [17], etc. Mechanical methods can also be employed to separate the cellulose fibers from RHs, such as using decorticating machines, steam explosion, Tilby process [18].

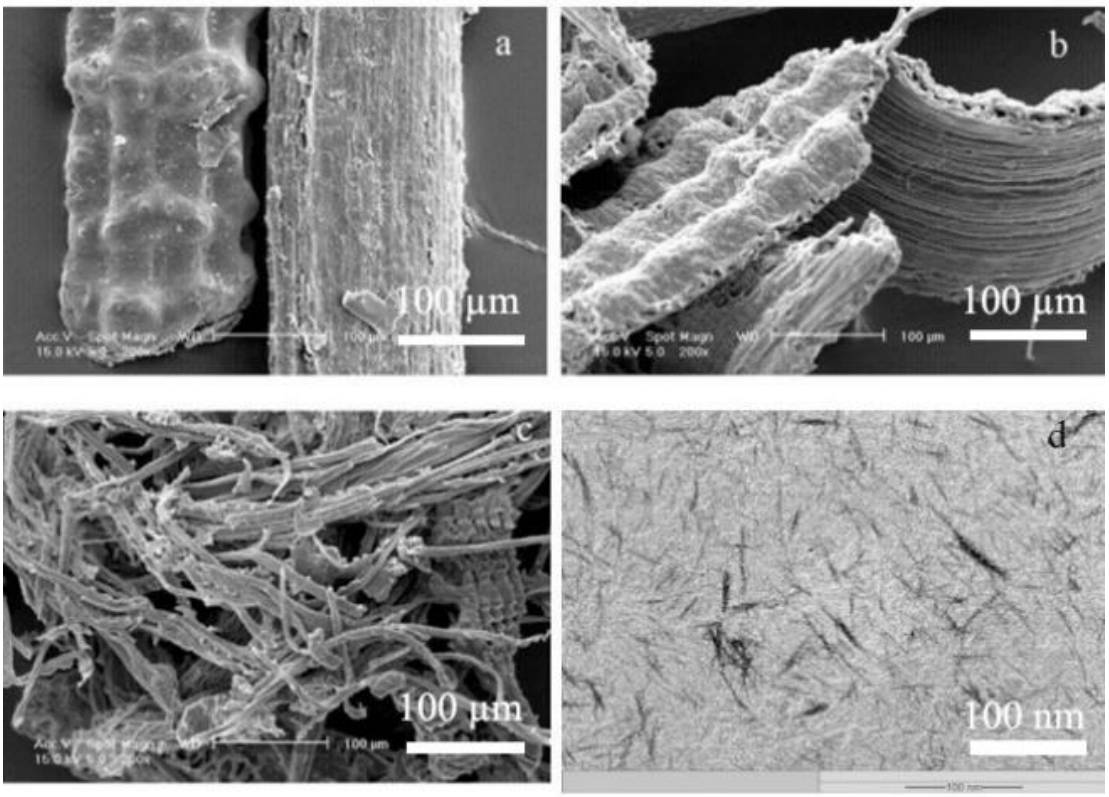

Figure 1. Scanning electron micrographs of (a) untreated RH fibers, (b) alkali-treated RH fibers, and (c) bleached RH fibers. (d) Transmission electron micrograph from a diluted suspension of cellulose nanocrystals extracted from RH fibers [19].

The extracted fibers from RHs could be mixed with polymers to make composites with improved mechanical performance. Garcia et al. [20] blended biodegradable poly(lactic acid) (PLA) with annually grown fibers (kenaf and RHs). The results showed that the biodegradability, mechanical properties, and flame retardant performance of the composites were improved. The improved composites could be used for structural, civil, automobile, and sporting goods applications. Xu et al. [21] used natural fibers from various biomasses including RHs, rice straws, bagasse, and pine, to make 13 different PVC based composites and tested their properties. The results showed that the composites had low absorption rates and a better dimensional stability in

water. It suggested that PVC filled with natural fibers had the properties comparable with those of PVC/wood composites [21].

1.2.3 Fossil Fuel Alternatives

Alternative energy has recently attracted much attention because of the need for clean power production. Syngas and biofuels should be popular substitute fuel resources, because they are environmentally friendly and inexpensive. The syngas extracted from RHs has been explored via gasification. The gas compositions are shown in Table 1 [22]. Note that H_2 and CH_4 have potential as renewable fuels. In the gasification process, there are two types of reactors, fluid bed reactor and tube reactor [23]. The typical temperature is 700 to 1000 ℃ and typical equivalence ratio 0.22-0.34 [24]. And the selected catalyst usually dictates the quality of the synthesized syngas. It was reported that different catalysts influence the syngas compositions. Kuo et al. [25] explored how different catalysts could affect the reaction. Alkali catalysts promoted the rate of gasification and increased the hydrogen concentration in the syngas. Nickel based catalysts were also quite effective for hydrogen generation [26].

Table 1. Gas composition I gasifier by random sampling [22].

Temperature (°C)		730	730	750	760	760	790	820	820	830	830	830
Gas Composition (%)	CO_2	15.4	16.2	16.0	15.5	15.3	15.7	14.6	15.3	15.1	14.5	15.3
	CO	19.0	18.6	17.4	18.7	15.4	15.9	15.8	16.5	16.5	15.6	16.1
	CH_4	6.8	7.3	8.0	7.3	8.8	6.8	5.0	6.7	7.5	8.4	4.1
	C_nH_m	1.7	1.6	1.6	1.6	1.5	1.5	1.4	1.3	1.5	1.0	1.2
	H_2	3.7	1.4	1.6	1.4	0.4	2.3	7.1	3.2	2.5	1.5	7.7
	N_2	51.7	53.5	54.3	54.3	56.9	56.5	54.5	56.3	55.6	57.5	53.9
	O_2	1.7	1.4	1.1	1.2	1.7	1.3	1.6	2.0	1.2	1.5	1.6
Gas Heating Value (MJ N m^{-3})		6.1	6.1	6.2	6.2	6.1	4.7	5.4	5.7	6.0	5.8	5.1

Bio-fuel is expected to play a significant role in fuel market because of its environmentally friendly nature and its renewability as opposed to fossil fuels. The extraction of bio-ethanol and bio-oil from RHs have attracted high interest because of the high lignocellulose content and the low price of RHs [27], and have achieved a yield of 13.9% and 16.1%, respectively [28].

Generally, the production of bio-ethanol consists of three procedures. Firstly, RHs are treated with acid. For cellulose, typically a diluted acid pretreatment is adopted, and for hemicellulose, a concentrated acid pretreatment is preferred. Then an assayed enzyme is mixed with the pretreated RHs to induce hydrolysis. This is also called the saccharification process, in which the biomass is changed to monomeric sugars. At last, fermentation is employed to yield ethanol.

Bio-oil is another bio-fuel product, which is made via pyrolysis. The main components of bio-oil were analyzed by Zheng et al. [27c] and listed in Table 2. Two types of reactors are used for

making bio-oil: fluidized bed reactors and fixed reactors. Because RHs contain a high concentration of various organic components, they will be pyrolyzed and degraded at different rates. To maintain a high efficiency of degradation, fast pyrolysis could be employed [29]. The entire system is shown in Figure 2 [30].

Table 2. Composition of bio-oil from RHs [27c].

Composition	wt. %
Formic acid	7.69
β-Hydroxybutyric acid	2.31
Toluene	5.00
Benzoic acid,3-methyl-	1.15
1,2-Benzenedicarboxylic acid	1.22
2-Cyclopentane-1-one, 3-methyl-	1.42
4H-Pyran-4-one, 2,6-dimethyl-	2.15
Acetophenone, 1-(4-hydroxy-3-methoxy)	1.00
Benzaldehyde,2-hydroxyl	1.85
Benzaldehyde,3,5-dimethyl-4-hydroxyl	1.92

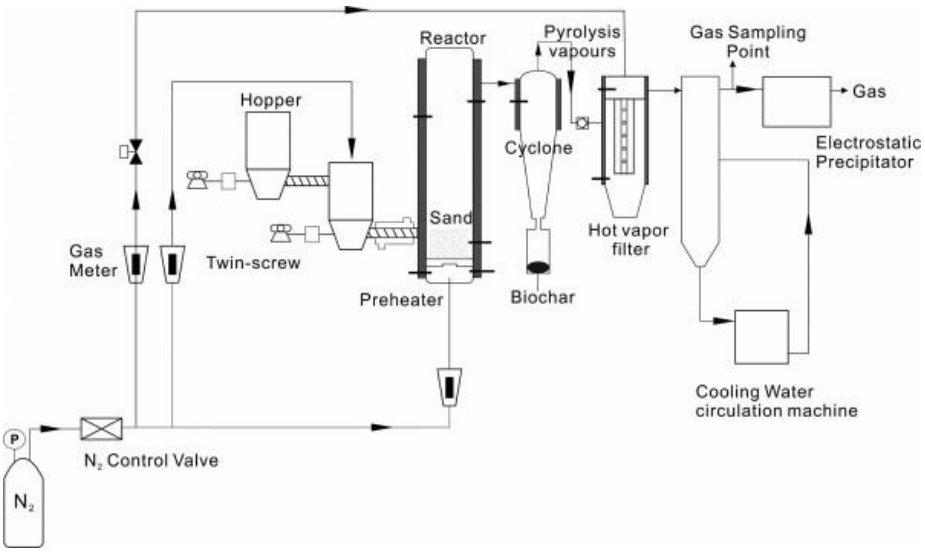

Figure 2. A representative fluidized-bed reactor fast pyrolysis system [30].

1.3 Construction Materials

The manufacture of existing building materials including concrete, particle boards, and bricks consumes a large amount of natural resources and causes various environmental issues primarily because of mining and air pollution [31]. Recycling bio wastes like RHs as construction materials is an attractive alternative because of the possible reduction in both energy and raw materials used [31].

The relatively low density of RHs was utilized by adding RHs to concrete to decrease thermal conductivity. RHs were added to concrete up to 30 wt. %. The decreased density lowered the thermal conductivity from ca. 1.54 to 0.71 W/mK. Although the compressive strength of the RHs filled concreate decreased from 37.5 to 17.6 MPa, the concrete was sufficient for practical applications [32].

With an increasing demand for wood construction materials, RHs are one of many agricultural byproducts that are being investigated for the manufacture of particle boards [31]. Particle boards were made from a 30 wt. % RHs and 70 wt. % wood (with urea-formaldehyde and phenol-formaldehyde resins) [33]. However, formaldehyde is expensive and brings health concerns. It is highly desirable to replace formaldehyde in particle board manufacturing. Soybean protein concentrate (SPC) was successfully used to bind RHs to form particle boards without the use of petrochemical derived resins [34]. Proteins functioning as adhesives is of interest because they are one of the most abundant and least expensive biologically derived feedstock [35]. Particle boards was initially prepared by blending RHs with home-made SPC adhesive (10 wt. %). Then the mixtures were dried at 70°C until 40 % moistures was reached. The balanced mixtures were pressed into particle board 10 minutes at 140 ºC under a pressure of 2.9 MPa [36]. The particles boards made of H_2O_2 bleached RHs and SPC exhibited an increased modulus of rupture and

modulus of elasticity [36]. The RH particle boards satisfy the US standard ANSI/A208.1 requirements for M1, MS, and M2-grade medium-density particleboards [36]. Although the particle boards from RHs do not display the same level of strength as the ones made of wood, they have unique properties. For example, the particle board made of a mixture of RHs and sawdust exhibited more effective sound absorbing performance than the commercial gypsum-fiber boards [37].

Lightweight bricks could be prepared by incorporating RHs into building materials. High strength lightweight bricks are now preferred for building design. They are lighter than traditional bricks, and the increased percentage of porosity also brings better thermal insulation properties than traditional bricks. Overall, experimental results showed that the lightweight bricks containing RHs possessed lower cost and weight, making them a good choice for construction applications [38]. Although the compressive strength was decreased with addition of RHs, it also could full fill the requirements respect to light weight bricks for construction work at the high temperature (1100 °C) [38] . The sintering method is the main approach to produce RHs-containing light weight bricks, and the whole process is shown in Figure 3 [39].

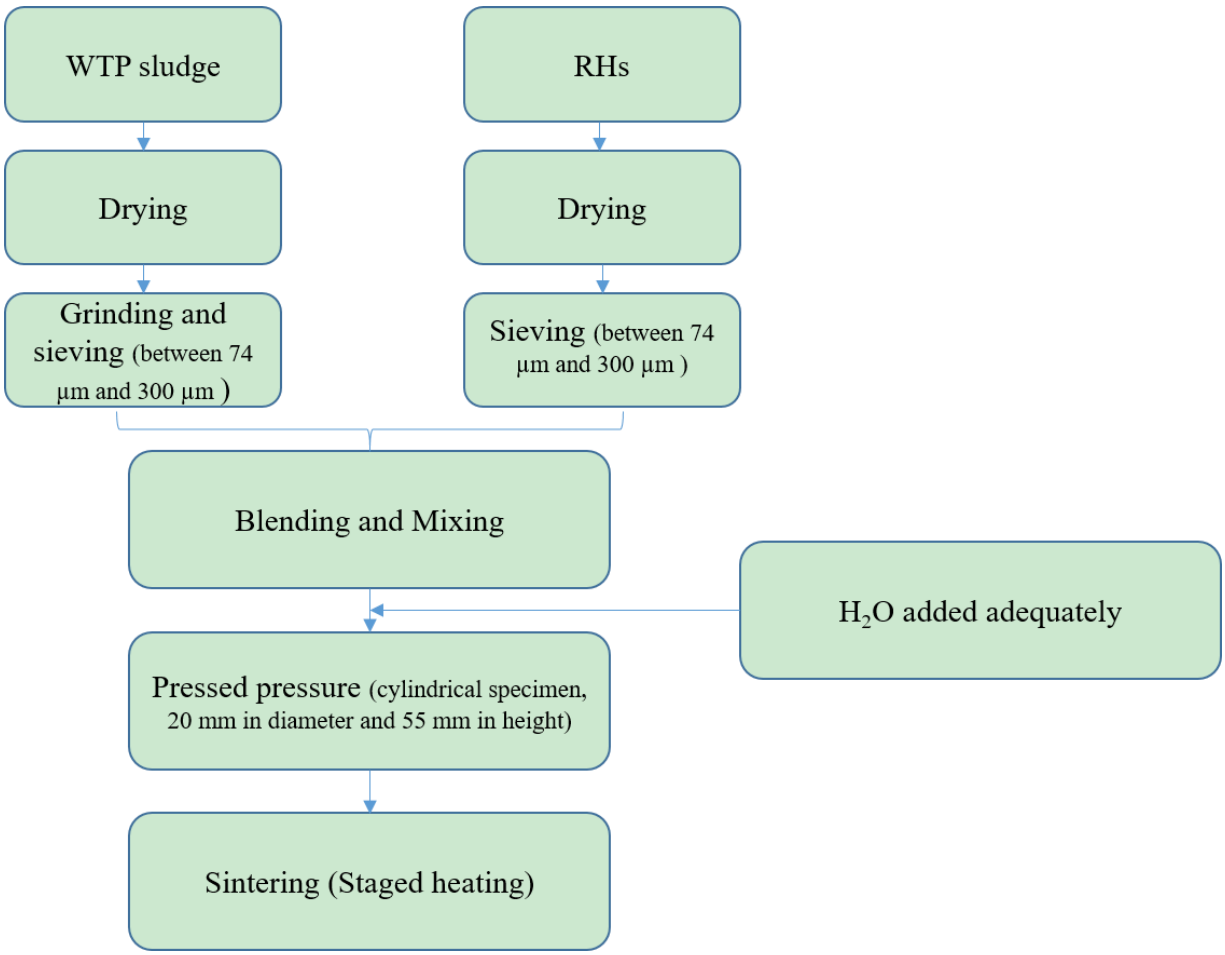

Figure 3. Sinter method for the preparation of lightweight bricks 39.

1.4 Composite Materials

RHs have recently attracted high interest as a filler for various composites. Fillers play an important role in modifying polymers to achieve desired properties and reducing the cost of composites [40]. Their abundance and biodegradability make RHs an attractive and economical material for fabricating composites.

Commodity polymers, such as polypropylene (PP), polyethylene (PE), polystyrene, etc. are widely used in our daily life because of their low cost, high process ability, and sufficiently high properties [41]. However, they are not degradable, remaining in the environment for a very long period of time. They also releases toxic gases upon combustion. RHs can be added into commodity

polymers to minimize such issues. RHs can also be incorporate into polymers to increase frictional properties for certain applications such as PP, PE [42]. For example, polyoxymethylene (POM) composites with 5 wt. % low-density polyethylene (LDPE) and 5 wt. % RHs exhibited better mechanical strength compared to neat POM [43].

RHs can be used as a filler for rubber composites as well. RHs were used in recycled acrylo nitrile butadiene rubber (NBRr) for nitrile glove applications [44]. This is an attractive composite using both a natural filler and a recycled material. It was reported that gamma-amino-propyltrimethoxysilane can effectively treat RHs, generating a more effective reinforcer. The composites containing treated RHs exhibited a higher tensile strength and modulus, but lower elongation break than the ones containing untreated RHs [44]. In addition, acetylation treated RHs blend with polystyrene/styrene butadiene rubber were effective in reducing the percentage of water absorption, because the acetyl groups reduced the hygroscopicity of the RHs [45].

1.5 Sorption of RH applications

RHs are an effective, safe, low-cost agent to sorb metals [46], oil [47], toxics [46b, 48], and dyes [49] from the environment. The earlier researches suggested that both the inorganic silica and organic lignocellulose in RHs were closely related to the sorption capability [46a, 48, 50]. The sorption process was assumed to be spontaneous and endothermic if the RHs were not treated or modified [46a, 51], as the sorption occurred at the surface rather than throughout the whole RH [46a]. RHs sorption was assessed under various parameters to observe the highest yielding sorption conditions, as well as most rapid rate [46a, 47-48, 50-52]. The untreated RHs and treated RHs exhibited different adsorption performances.

Without any treatment, the RHs sorption performance for silver [46a], arsenic [52], lead [46b], and oils [47a] was examined in different experiments. All except oil sorption supported that RHs had the

capacity to sorb sufficiently for further consideration of applications [47a]. Because RHs have a low water to oil sorption ratio, the capacity to adsorb diesel, crude oils, new engine and used engine oils was low and unsuccessful [47a]. Four factors could tune the performance of untreated RHs: optimal pH value, moderate concentration (amounts of RHs and metal ions), enough equilibrium time, and temperature [46, 52].

Acid or alkali chemical treatment [48-49, 53] or thermal treatment [47b, 47c, 53] of RHs can help improve the sorption performance of RHs particularly for metal ions, including shortening equilibrium time and increasing pore volume. Same as the untreated RHs, the optimal pH and temperature also contribute to the sorption performance of the treated RHs [47c, 48-49].

Overall, treated RHs exhibit higher sorption performance but untreated RHs are more cost-effective. Using RHs to as a sorb agent is highly beneficial for the environment, since this is a process to use a biowaste to improve environment.

1.6 Power Generation

Generation of power using RHs was proved successful, yet very not easy to commercialize. Investigations were conducted on profitability, cost analysis, cost effectiveness, and the performance of RHs for power generation since the late 1960's [54]. It was reported that RHs could be used to balance undesired carbon dioxide emissions from energy producing systems including gasification and combustion [55] . RH power generation could be profitable within larger plants solely if the surplus electricity generated is sold directly to the national power grid.

The gasification process converts organic carbonaceous materials into CO, H_2, and CO_2 by heating them to temperatures above 700 °C with controlled ratios of O_2, and produces a synthetic fuel. Biomass gasification and power generation technologies have been studied since as early as 1960, and RHs gasification has developed significantly since then. According to the collected data,

the gasification temperature is related to the heating value returned. The moisture content of RHs has a great influence on the system and should be preheated to be maintained below 15% to obtain optimum results [56]. It was found that optimum excessive air ratios for the gasification process range from 0.3-0.6 and has a significant impact on the efficiency of the gasification results. The study concluded that a continuous power generation of 10 kW was achieved [57].

In comparison with other thermo-chemical power conversion technologies, combustion is proven to be the most efficient [58]. Recently, evaluating the characteristics of generating power through combustion of RHs alone, as well as being co-fired with equalizing alternatives [58b, 59], such as sugarcane bagasse and coal. The results showed that the co-fired RHs, mixed with other components such as coal and sugarcane bagasse, performed better than combusting RHs alone. Co-fired RHs had lower NO emissions and less O_2 production in flue gas than when firing 100% RHs. Fluid bed combustor (FBC) power generation proved to be a very promising technique, returning combustion efficiencies ranging from 95.0-99.1% between different FBCs.

1.7 Comprehensive Utilization of RHs

The contents in RHs are complex with multiple possible applications. However, researchers usually focus on one component during their exploration For example, silica is usually the focus on research while organic lignocellulose was typically ignored. Comprehensive strategies have been recently explored. The goal is to increase the utilization efficiency and products diversity of RH biomass. The basic procedures of the comprehensive strategy is to start with a chemical pretreatment, such as acid or alkali hydrolysis. By multiple treatments, one or more products can be obtained in every reaction stage. For example, Zhang et al. [60] used acid hydrolysis as the main treatment to obtain D-xylose, lignin, ethanol, and superfine silica from RHs. Figure 4 shows the

schematic process of extracting several products from RHs. This kind of strategy improves the utilization efficiency of RH biomass, which is beneficial and highly desirable.

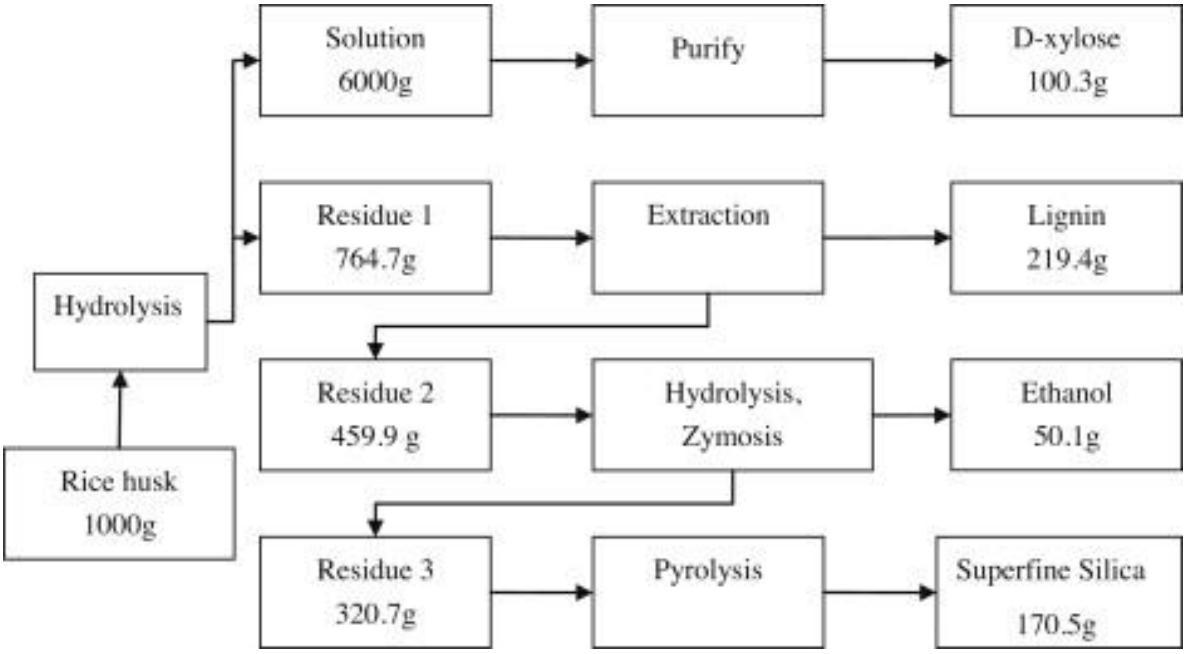

Figure 4. Technological process of comprehensively utilizing RHs 60.

1.8 Conclusion

In brief, RHs are one of abundant biomasses. The remarkable physical and chemical properties of amorphous silica and lignocellulose give RHs a wide variety of applications including chemical production, construction materials, sorption materials, power generation, and composite materials. Biomass comprehensive application strategy is a new concept for solving the problem of low utilization efficiency and product diversity, which is also the goal of this thesis. Herein,

Chapter 2 reports the extraction of highly active amorphous silica nanoparticles from RHs for the synthesis of green phosphors, which have applications including plasma displays and fluorescent lamps. Chapter 3 reports the exploration to obtain both silica nanoparticles and lignocellulose from RHs. The lignocellulose could be extracted from RHs using an ionic liquid to prepare aerogels via a freeze-thaw process. By converting the lignocellulose aerogel to be

hydrophobic through surface treatment, it could find applications in oil spill remediation. Carbon aerogel could be further obtained from the lignocellulose aerogel via high temperature calcination. Silica nanoparticles were also obtained by calcining the RH residue after ionic liquid extraction. The obtained silica can be applied for various applications. Chapter 4 gives a summary of this thesis and an outlook.

References

1. Gadde, B.; Bonnet, S.; Menke, C.; Garivait, S., Air pollutant emissions from rice straw open field burning in India, Thailand and the Philippines. *Environmental Pollution* **2009,** *157* (5), 1554-1558.
2. Chen, H.; Wang, W.; Martin, J. C.; Oliphant, A. J.; Doerr, P. A.; Xu, J. F.; DeBorn, K. M.; Chen, C.; Sun, L., Extraction of lignocellulose and synthesis of porous silica nanoparticles from rice husks: a comprehensive utilization of rice husk biomass. *ACS Sustainable Chemistry & Engineering* **2012,** *1* (2), 254-259.
3. Balathanigaimani, M. S.; Kang, H.-C.; Shim, W.-G.; Kim, C.; Lee, J.-W.; Moon, H., Preparation of powdered activated carbon from rice husk and its methane adsorption properties. *Korean Journal of Chemical Engineering* **2006,** *23* (4), 663-668.
4. Jüntgen, H., Activated carbon as catalyst support: a review of new research results. *Fuel* **1986,** *65* (10), 1436-1446.
5. Sircar, S.; Golden, T.; Rao, M., Activated carbon for gas separation and storage. *Carbon* **1996,** *34* (1), 1-12.
6. Ali, I., The quest for active carbon adsorbent substitutes: inexpensive adsorbents for toxic metal ions removal from wastewater. *Separation & Purification Reviews* **2010,** *39* (3-4), 95-171.
7. Haykiri-Acma, H.; Yaman, S.; Kucukbayrak, S., Gasification of biomass chars in steam–nitrogen mixture. *Energy Conversion and Management* **2006,** *47* (7), 1004-1013.
8. Lanzetta, M.; Di Blasi, C., Pyrolysis kinetics of wheat and corn straw. *Journal of Analytical and Applied Pyrolysis* **1998,** *44* (2), 181-192.
9. Minkova, V.; Razvigorova, M.; Bjornbom, E.; Zanzi, R.; Budinova, T.; Petrov, N., Effect of water vapour and biomass nature on the yield and quality of the pyrolysis products from biomass. *Fuel Processing Technology* **2001,** *70* (1), 53-61.
10. Zhu, K.; Fu, H.; Zhang, J.; Lv, X.; Tang, J.; Xu, X., Studies on removal of NH 4+-N from aqueous solution by using the activated carbons derived from rice husk. *Biomass and bioenergy* **2012,** *43*, 18-25.
11. Yao, S.; Zhang, J.; Shen, D.; Xiao, R.; Gu, S.; Zhao, M.; Liang, J., Removal of Pb (II) from water by the activated carbon modified by nitric acid under microwave heating. *Journal of colloid and interface science* **2016,** *463*, 118-127.
12. Mashhadi, S.; Sohrabi, R.; Javadian, H.; Ghasemi, M.; Tyagi, I.; Agarwal, S.; Gupta, V. K., Rapid removal of Hg (II) from aqueous solution by rice straw activated carbon prepared by microwave-assisted H 2 SO 4 activation: Kinetic, isotherm and thermodynamic studies. *Journal of Molecular Liquids* **2016,** *215*, 144-153.
13. Lu, C.-Y.; Wey, M.-Y.; Chuang, K.-H., Catalytic treating of gas pollutants over cobalt catalyst supported on porous carbons derived from rice husk and carbon nanotube. *Applied Catalysis B: Environmental* **2009,** *90* (3), 652-661.
14. (a) Ganesan, A.; Mukherjee, R.; Raj, J.; Shaijumon, M. M., Nanoporous rice husk derived carbon for gas storage and high performance electrochemical energy storage. *Journal of Porous Materials* **2014,** *21* (5), 839-847; (b) Chen, H.; Wang, H.; Xue, Z.; Yang, L.; Xiao, Y.; Zheng, M.; Lei, B.; Liu, Y.; Sun, L., High hydrogen storage capacity of rice hull based porous carbon. *international journal of hydrogen energy* **2012,** *37* (24), 18888-18894.
15. Reddy, N.; Yang, Y., Biofibers from agricultural byproducts for industrial applications. *TRENDS in Biotechnology* **2005,** *23* (1), 22-27.

16. Nguyen, T.-D.; Hamad, W. Y.; MacLachlan, M. J., Tuning the iridescence of chiral nematic cellulose nanocrystals and mesoporous silica films by substrate variation. *Chemical Communications* **2013,** *49* (96), 11296-11298.
17. Adolfsson, K. H.; Hassanzadeh, S.; Hakkarainen, M., Valorization of cellulose and waste paper to graphene oxide quantum dots. *Rsc Advances* **2015,** *5* (34), 26550-26558.
18. (a) Focher, B.; Marzetti, A.; Marsano, E.; Conio, G.; Tealdi, A.; Cosani, A.; Terbojevich, M., Regenerated and graft copolymer fibers from steam-exploded wheat straw: Characterization and properties. *Journal of Applied Polymer Science* **1998,** *67* (6), 961-974; (b) Gollapalli, L. E.; Dale, B. E.; Rivers, D. M., *Predicting digestibility of ammonia fiber explosion (AFEX)-treated rice straw*. Springer: 2002; (c) Tilby, S. E., Method and apparatus for processing sugarcane. Google Patents: 1971.
19. Johar, N.; Ahmad, I.; Dufresne, A., Extraction, preparation and characterization of cellulose fibres and nanocrystals from rice husk. *Industrial Crops and Products* **2012,** *37* (1), 93-99.
20. Garcia, M.; Garmendia, I.; Garcia, J., Influence of natural fiber type in eco-composites. *Journal of Applied Polymer Science* **2008,** *107* (5), 2994-3004.
21. Xu, Y.; Wu, Q.; Lei, Y.; Yao, F.; Zhang, Q., Natural Fiber Reinforced Poly(vinyl chloride) Composites: Effect of Fiber Type and Impact Modifier. *Journal of Polymers and the Environment* **2008,** *16* (4), 250-257.
22. Yin, X. L.; Wu, C. Z.; Zheng, S. P.; Chen, Y., Design and operation of a CFB gasification and power generation system for rice husk. *Biomass & Bioenergy* **2002,** *23* (3), 181-187.
23. Bhat, A.; Bheemarasetti, J. V. R.; Rao, T. R., Kinetics of rice husk char gasification. *Energy Conversion and Management* **2001,** *42* (18), 2061-2069.
24. Zhao, Y.; Sun, S.; Tian, H.; Qian, J.; Su, F.; Ling, F., Characteristics of rice husk gasification in an entrained flow reactor. *Bioresource Technology* **2009,** *100* (23), 6040-6044.
25. Kuo, H. P.; Pan, S. M.; Hsu, H. T., Comparisons of the hydrogen-rich syngas compositions from wet rice husk slurry steam reforming reactions using different catalysts. *Biomass & Bioenergy* **2011,** *35* (7), 3025-3031.
26. (a) Le, D. D.; Xiao, X.; Morishita, K.; Takarada, T., Biomass gasification using nickel loaded brown coal char in fluidized bed gasifier at relatively low temperature. *Journal of Chemical Engineering of Japan* **2009,** *42* (1), 51-57; (b) Bona, S.; Guillén, P.; Alcalde, J. G.; Garcá, L.; Bilbao, R., Toluene steam reforming using coprecipitated Ni/Al catalysts modified with lanthanum or cobalt. *Chemical Engineering Journal* **2008,** *137* (3), 587-597; (c) Wang, T.; Chang, J.; Wu, C.; Fu, Y.; Chen, Y., The steam reforming of naphthalene over a nickel–dolomite cracking catalyst. *Biomass and Bioenergy* **2005,** *28* (5), 508-514.
27. (a) Saha, B. C.; Iten, L. B.; Cotta, M. A.; Wu, Y. V., Dilute acid pretreatment, enzymatic saccharification, and fermentation of rice hulls to ethanol. *Biotechnology Progress* **2005,** *21* (3), 816-822; (b) Zheng, J.-l.; Zhu, X.-f.; Guo, Q.-x.; Zhu, Q.-s., Thermal conversion of rice husks and sawdust to liquid fuel. *Waste Management* **2006,** *26* (12), 1430-1435; (c) Zheng, J.-l., Bio-oil from fast pyrolysis of rice husk: Yields and related properties and improvement of the pyrolysis system. *Journal of Analytical and Applied Pyrolysis* **2007,** *80* (1), 30-35; (d) Chen, T.; Wu, C.; Liu, R., Steam reforming of bio-oil from rice husks fast pyrolysis for hydrogen production. *Bioresource Technology* **2011,** *102* (19), 9236-9240.
28. Abbas, A.; Ansumali, S., Global potential of rice husk as a renewable feedstock for ethanol biofuel production. *Bioenergy Research* **2010,** *3* (4), 328-334.

29. Bridgwater, A., Principles and practice of biomass fast pyrolysis processes for liquids. *Journal of Analytical and Applied Pyrolysis* **1999,** *51* (1), 3-22.
30. Chen, T.; Wu, C.; Liu, R.; Fei, W.; Liu, S., Effect of hot vapor filtration on the characterization of bio-oil from rice husks with fast pyrolysis in a fluidized-bed reactor. *Bioresource Technology* **2011,** *102* (10), 6178-6185.
31. Safiuddin, M.; Jumaat, M. Z.; Salam, M.; Islam, M.; Hashim, R., Utilization of solid wastes in construction materials. *International Journal of Physical Sciences* **2010,** *5* (13), 1952-1963.
32. Sisman, C.; Gezer, E.; Kocaman, I., Effects of organic waste (rice husk) on the concrete properties for farm buildings. *Bulgarian Journal of Agricultural Science* **2011,** *17* (1), 40-48.
33. Ayrilmis, N.; Kwon, J. H.; Han, T. H., Effect of resin type and content on properties of composite particleboard made of a mixture of wood and rice husk. *International Journal of Adhesion and Adhesives* **2012,** *38*, 79-83.
34. Ciannamea, E. M.; Stefani, P. M.; Ruseckaite, R. A., Medium-density particleboards from modified rice husks and soybean protein concentrate-based adhesives. *Bioresource Technology* **2010,** *101* (2), 818-825.
35. Cheng, H.; Wartelle, L. H.; Klasson, K. T.; Edwards, J. C., Solid-state NMR and ESR studies of activated carbons produced from pecan shells. *Carbon* **2010,** *48* (9), 2455-2469.
36. Yat, S. C.; Berger, A.; Shonnard, D. R., Kinetic characterization for dilute sulfuric acid hydrolysis of timber varieties and switchgrass. *Bioresource Technology* **2008,** *99* (9), 3855-3863.
37. Matsushita, Y.; Yasuda, S., Preparation of anion-exchange resins from pine sulfuric acid lignin, one of the acid hydrolysis lignins. *Journal of Wood Science* **2003,** *49* (5), 423-429.
38. Chiang, K. Y.; Chou, P. H.; Chien, K. L.; Chen, J. L.; Wu, C. C., Novel Lightweight Building Bricks Manufactured from Water Treatment Plant Sludge and Agricultural Waste. *Journal of Residuals Science & Technology* **2009,** *6* (4), 185-191.
39. Chiang, K.-Y.; Chou, P.-H.; Hua, C.-R.; Chien, K.-L.; Cheeseman, C., Lightweight bricks manufactured from water treatment sludge and rice husks. *Journal of hazardous materials* **2009,** *171* (1), 76-82.
40. Kord, B., NANOFILLER REINFORCEMENT EFFECTS ON THE THERMAL, DYNAMIC MECHANICAL, AND MORPHOLOGICAL BEHAVIOR OF HDPE/RICE HUSK FLOUR COMPOSITES. *Bioresources* **2011,** *6* (2), 1351-1358.
41. Arora, A.; Padua, G., Review: nanocomposites in food packaging. *Journal of Food science* **2010,** *75* (1), R43-R49.
42. (a) Yang, H.-S.; Kim, H.-J.; Son, J.; Park, H.-J.; Lee, B.-J.; Hwang, T.-S., Rice-husk flour filled polypropylene composites; mechanical and morphological study. *Composite Structures* **2004,** *63* (3), 305-312; (b) Hardinnawirda, K. The effect of rice husks as filler in polymer matrix composites. Universiti Malaysia Pahang, 2012; (c) Kim, H.-S.; Yang, H.-S.; Kim, H.-J.; Park, H.-J., Thermogravimetric analysis of rice husk flour filled thermoplastic polymer composites. *Journal of Thermal Analysis and Calorimetry* **2004,** *76* (2), 395-404.
43. Li, K.; Xiang, D.; Lei, X., Green and self-lubricating polyoxymethylene composites filled with low-density polyethylene and rice husk flour. *Journal of Applied Polymer Science* **2008,** *108* (5), 2778-2786.
44. Santiagoo, R.; Ismail, H.; Hussin, K., Mechanical properties, water absorption, and swelling behaviour of rice husk powder filled polypropylene/recycled acrylonitrile butadiene rubber (PP/NBRr/RHP) biocomposites using silane as a coupling agent. *BioResources* **2011,** *6* (4), 3714-3726.

45. Zurina, M.; Ismail, H.; Bakar, A. A., Rice husk powder-filled polystyrene/styrene butadiene rubber blends. *Journal of Applied Polymer Science* **2004,** *92* (5), 3320-3332.
46. (a) Zafar, S.; Khalid, N.; Mirza, M. L., Potential of rice husk for the decontamination of silver ions from aqueous media. *Separation Science and Technology* **2012,** *47* (12), 1793-1801; (b) Singha, B.; Das, S. K., Removal of Pb (II) ions from aqueous solution and industrial effluent using natural biosorbents. *Environmental science and pollution research* **2012,** *19* (6), 2212-2226.
47. (a) Ali, N.; El-Harbawi, M.; Jabal, A. A.; Yin, C.-Y., Characteristics and oil sorption effectiveness of kapok fibre, sugarcane bagasse and rice husks: oil removal suitability matrix. *Environmental technology* **2012,** *33* (4), 481-486; (b) Kenes, K.; Yerdos, O.; Zulkhair, M.; Yerlan, D., Study on the effectiveness of thermally treated rice husks for petroleum adsorption. *Journal of Non-Crystalline Solids* **2012,** *358* (22), 2964-2969; (c) Angelova, D.; Uzunov, I.; Uzunova, S.; Gigova, A.; Minchev, L., Kinetics of oil and oil products adsorption by carbonized rice husks. *Chemical Engineering Journal* **2011,** *172* (1), 306-311.
48. Hsu, S.-T.; Pan, T.-C., Adsorption of paraquat using methacrylic acid-modified rice husk. *Bioresource technology* **2007,** *98* (18), 3617-3621.
49. Chakraborty, S.; Chowdhury, S.; Saha, P. D., Adsorption of crystal violet from aqueous solution onto NaOH-modified rice husk. *Carbohydrate Polymers* **2011,** *86* (4), 1533-1541.
50. (a) Low, K. S.; Lee, C. K.; Wong, S. Y.; Tang, P. L., Metal soprtion enhancement of rice hull through chemical modification. *Environmental Technology* **2000,** *21* (11), 1239-1243; (b) Chakraborty, S.; Chowdhury, S.; Das Saha, P., Adsorption of Crystal Violet from aqueous solution onto NaOH-modified rice husk. *Carbohydrate Polymers* **2011,** *86* (4), 1533-1541.
51. Singha, B.; Das, S. K., Removal of Pb(II) ions from aqueous solution and industrial effluent using natural biosorbents. *Environmental Science and Pollution Research* **2012,** *19* (6), 2212-2226.
52. Amin, M. N.; Kaneco, S.; Kitagawa, T.; Begum, A.; Katsumata, H.; Suzuki, T.; Ohta, K., Removal of arsenic in aqueous solutions by adsorption onto waste rice husk. *Industrial & engineering chemistry research* **2006,** *45* (24), 8105-8110.
53. Low, K.; Lee, C.; Wong, S.; Tang, P., Metal soprtion enhancement of rice hull through chemical modification. *Environmental technology* **2000,** *21* (11), 1239-1244.
54. Yin, X. L.; Wu, C. Z.; Zheng, S. P.; Chen, Y., Design and operation of a CFB gasification and power generation system for rice husk. *Biomass and Bioenergy* **2002,** *23* (3), 181-187.
55. Thao, P. T. M.; Kurisu, K. H.; Hanaki, K., Evaluation of strategies for utilizing rice husk based on life cycle cost analysis in relation to Greenhouse Gas emissions in An Giang province, Vietnam. *biomass and bioenergy* **2012,** *37*, 122-131.
56. Wu, C.-z.; Yin, X.-l.; Ma, L.-l.; Zhou, Z.-q.; Chen, H.-p., Operational characteristics of a 1.2-MW biomass gasification and power generation plant. *Biotechnology advances* **2009,** *27* (5), 588-592.
57. Yoon, S. J.; Son, Y.-I.; Kim, Y.-K.; Lee, J.-G., Gasification and power generation characteristics of rice husk and rice husk pellet using a downdraft fixed-bed gasifier. *Renewable Energy* **2012,** *42*, 163-167.
58. (a) Singh, R. I.; Mohapatra, S.; Gangacharyulu, D., Studies in an atmospheric bubbling fluidized-bed combustor of 10MW power plant based on rice husk. *Energy Conversion and Management* **2008,** *49* (11), 3086-3103; (b) Sathitruangsak, P.; Madhiyanon, T.; Soponronnarit, S., Rice husk co-firing with coal in a short-combustion-chamber fluidized-bed combustor (SFBC). *Fuel* **2009,** *88* (8), 1394-1402.
59. (a) Kuprianov, V. I.; Janvijitsakul, K.; Permchart, W., Co-firing of sugar cane bagasse with rice husk in a conical fluidized-bed combustor. *Fuel* **2006,** *85* (4), 434-442; (b) Madhiyanon, T.;

Sathitruangsak, P.; Soponronnarit, S., Co-firing characteristics of rice husk and coal in a cyclonic fluidized-bed combustor (Ψ-FBC) under controlled bed temperatures. *Fuel* **2011,** *90* (6), 2103-2112.
60. Zhang, H.; Ding, X.; Chen, X.; Ma, Y.; Wang, Z.; Zhao, X., A new method of utilizing rice husk: consecutively preparing d-xylose, organosolv lignin, ethanol and amorphous superfine silica. *Journal of hazardous materials* **2015,** *291*, 65-73.

Chapter 2. Synthesis of Green Phosphor from Highly Active Amorphous Silica Derived from Rice Husks

2.1 Introduction

Rice husks are one of the largest sources of biomass in the world because of the enormous amount of rice consumed globally every year [1]. In the past, RHs were mainly treated as a waste; they were often disposed of by open-field burning, especially in developing countries, leading to significant air pollution [2]. RHs contain two major components: silica (ca. 15-28 wt. %) and lignocellulose (LC, ca. 72-85 wt. %) [3], both of which can find a wide range of applications. For example, syngas and biofuel, which are promising power alternatives, can be synthesized from RH LC via hydrolysis and fermentation, respectively [4].Silica, the major inorganic component of RH, is an essential chemical widely used as a catalyst support [5], adsorption material [6], and raw material for various silicon-based chemicals [7]. This silica source is promising for industry applications because of the facile and low power consumption production, and low price. Several methods have been developed to prepare silica from RHs, including thermal decomposition method (calcination) [8], hydrothermal reaction [9], and fungus biotransformation method [10]. Direct calcination is usually preferred in industry due to its low cost. The purity of the silica derived from RHs could reach 99.8% after calcination [11]. This suggests that the RH silica can be a valid resource for many silica-related applications.

Recently, many new silicate applications were developed from RH silica. For example, silicate pigments of multiple colors, which can be applied for ceramic materials and glaze, were reported by doping silicates from RH silica with different elements [11]. Sodium silicate was also prepared from RH silica, which served as a solid catalyst for transesterification reaction of oil to biodiesel, and exhibited high performance [12]. Magnesium silicate synthesized from RH silica was

used to catalyze a ring-opening reaction to synthesize propranolol glycol from glycidol and 1-naphthol and achieved a conversion rate of 85% [13].

Phosphors have widespread application, including plasma display (PDP), phosphor thermometry, and fluorescent lamps [14]. While many natural phosphors have been discovered, with an increasing market demand for phosphorescent materials, developing methods to prepare artificial phosphors is necessary. For example, green artificial silicate phosphor can be made by doping Zn_2SiO_4 with Mn^{2+}, in which Mn^{2+} cations partly replace the positions of the Zn^{2+} cations, resulting in a broad emission band under UV light excitation [15]. Three common doping methods have been reported, including solid-state calcination [16], hydrothermal treatment [16-17] and sol-gel method [16, 18]. Demands for phosphors keep increasing, so facile process to prepare phosphors using inexpensive raw materials are highly desirable.

In this paper, we report our exploration to extract high purity amorphous silica from RHs by calcination and use the synthesized RH silica to make green phosphors. Various parameters were adjusted to achieve the highest luminescence. Considering this is a very facile method to synthesize phosphors at a low cost, it may be further developed for commercial production of phosphors for practical applications.

2.2 Experiment

2.2.1 Preparation of silica from RHs

The RH sample (from Rice Hull Specialty Products, Inc., Stuttgart, AR) was pretreated by 10% hydrochloric acid (HCl, 35%, Fisher Scientific) at 95 ℃ for 2 hours. The sample was rinsed by deionized water three times to eliminate the residual components. Then, it was dried in an oven at 80 ℃ for 24 hours. After the sample was completely dried, it was grinded for further use. A

sample of 3 g RH was treated in a tube furnace under air atmosphere at 700 ℃ for 2 hours.[5a, 8, 11] After that, 0.72 ± 0.02 g silica was obtained.

2.2.2 Preparation of $Zn_2SiO_4:Mn^{2+}$

The silica sample was mixed with zinc nitrate hexahydrate (99 %, Alfa Aesar, USA) and manganese (II) nitrate tetrahydrate (98 %, Alfa Aesar) in a mortar until all the powders were uniform. The concentration control of $Zn_2SiO_4:Mn^{2+}$ from 4% to 12%. Then the powder sample underwent calcination in a tube furnace under nitrogen atmosphere. The reacting temperature for each sample was controlled from 1000-1200 ℃, and the reaction last for 4 hours. The control phosphor samples were prepared by silicic acid [19] (99.9 %, Sigma-Aldrich, USA) or silica (99.5 %, 325 mesh, Alfa Aesar, USA) [20]. After the reaction, the samples were ground for further characterization.

2.2.3 Characterization

The silica sample and phosphor samples were characterized by X-ray diffraction (XRD; Bruker D2, 40 KV and 30 mA) using a graphite monochromator with Cu Kα radiation (λ=0.1540 nm). In order to analyze the surface area of RH silica, nitrogen adsorption-desorption isotherms was recorded by Quantachrome NOVA 2000e. And the specific surface area was calculated by Brunauer-Emmett-Teller (BET) theory. The excitation, decay lifetime, and emission spectra of the powder samples were measured using an Edinburgh Instruments FLS980 fluorometer system. For the absolute quantum yield (QY) measurements, and to compare the intensities between the samples, an integrating sphere was employed in the FLS980 fluorometer [21].

To be consistent, the sample weight (20 mg) and monochromator slit size (3 nm for both excitation and emission monochromators) were kept for all experiments. Photoluminescence (PL) spectra from 400-700 nm and excitation spectra of 235-325 nm were collected after diffuse

reflectance from the samples, relative to a non-absorbing standard at the excitation wavelength, and emission spectra were collected under the same conditions. QY was measured by finding the ratio of the area under the emission spectra to the difference in corrected area under the diffuse reflectance of the excitation spectra for the sample and the reference. It was calculated based on the equation below:

$$QY = \frac{NP_{emitted}}{NP_{absorbed}} = \frac{\int N_{em} d\lambda}{\int N_{abs} d\lambda} = \frac{A_{sample}}{A_{reference} - A_{sample}} \quad (1)$$

Including all the possible errors, such as reflectivity of the reference (< 3 %), particle size effects (< 2 %), and diffuse reflectance from the sample holder (< 3 %), the estimated error in QY was about 10 %. Similarly, the estimated fluctuation for excitation power was about 2 %. The excitation power was measured to be 6 mW.

2.3 Results and Discussion

Figure 5 shows the flow chart to prepare RH phosphor. The original RH treated by diluted HCl. Weighing 3 g treated RH into alumina crucible and the highly active amorphous silica was extracted from treated RH under air atmosphere at 700 ℃ for 2 hours. By mixing and grounding RH silica with $Zn(NO_3)_2 \cdot 6H_2O$ and $Mn(NO_3)_2 \cdot 4H_2O$, RH phosphor was obtained under N_2 atmosphere at 1200 ℃. Under UV light, the white powder of RH phosphor emitted intensive green light.

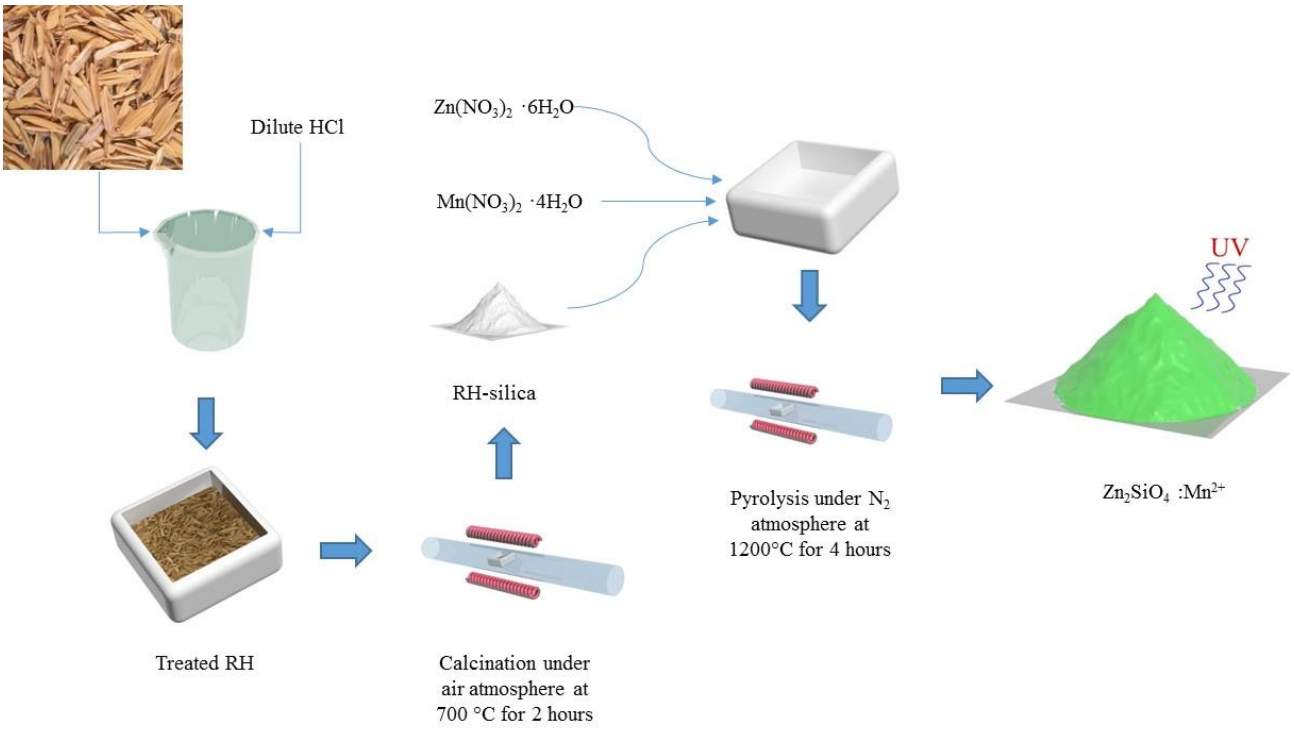

Figure 5. Steps to make RH-silica based green phosphors.

White silica powders were easily synthesized from the HCl pretreated RHs via calcination, as shown in Figure 6. The broad diffraction band from 15 °to 40 °in the XRD pattern in Figure 2 shows that the RH silica was amorphous, consistent with the literature [11], mainly because the HCl pretreatment eliminated metal ions, particularly K^+ cations, which could catalyze the melting of silica. The amorphous nature and high specific surface area (354.6 m^2/g) of RH silica indicate its high reactivity during the synthesis of silicate phosphors.

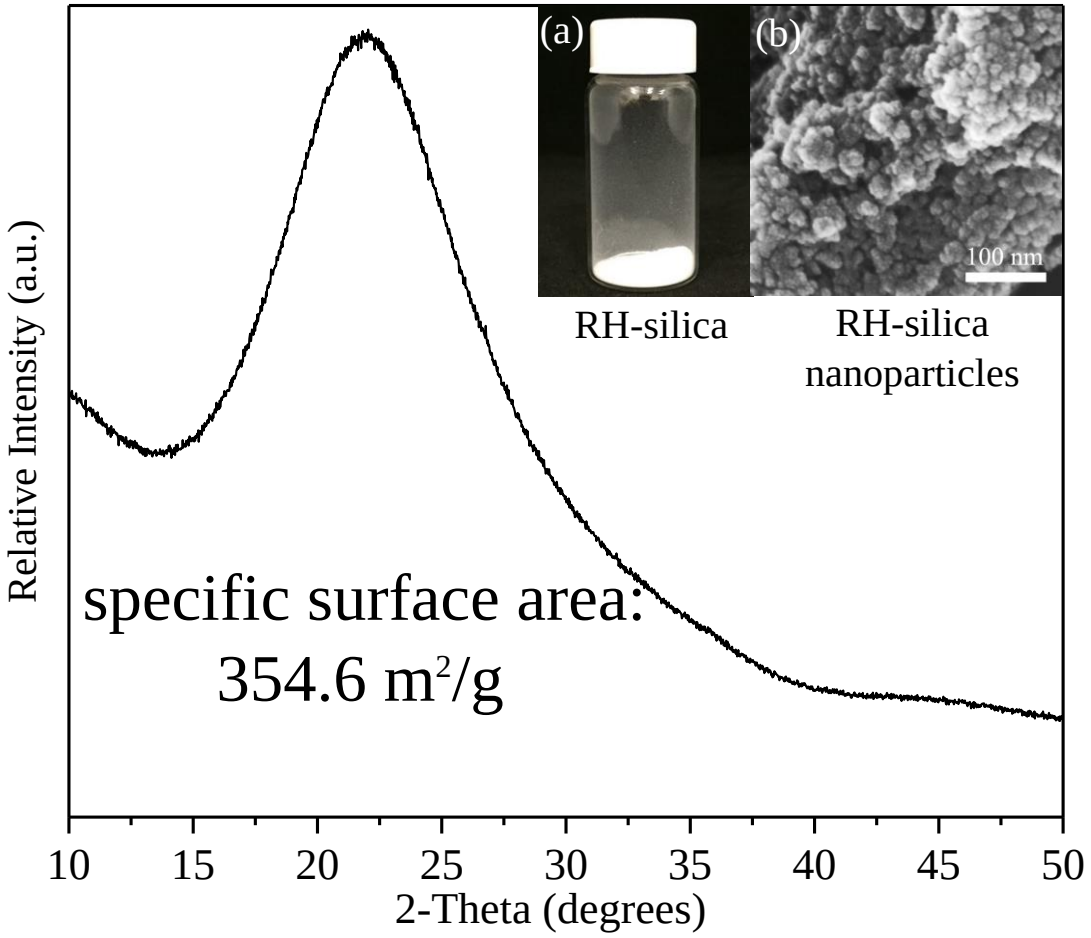

Figure 6. X-ray diffraction of the synthesized RH silica. The inset figure (a) is a digital picture of the sample; figure (b) is SEM of RH-silica nanoparticles

In commercial $Zn_2SiO_4:Mn^{2+}$ phosphor, the Mn^{2+} doping concentration is typically 8% (i.e., $Zn_2SiO_4:0.08Mn^{2+}$), as the $Zn_2SiO_4:Mn^{2+}$ phosphor usually exhibits the highest intensity at such as doping concentration [22]. As such, we adopt this doping concentration to explore the $Zn_2SiO_4:Mn^{2+}$ synthesized from RH silica under various temperatures.

The RH phosphor samples were prepared by high temperature pyrolysis, during which RH silica, $Zn(NO_3)_2 \cdot 6H_2O$, and $Mn(NO_3)_2 \cdot 4H_2O$ were mixed under nitrogen atmosphere at high conditioning temperatures (1000, 1100, and 1200 ℃) for 4 hours. The XRD patterns of

Zn_2SiO_4:0.08Mn^{2+} under different reaction temperatures are shown in Figure 7. All the patterns exhibit sharp and intense peaks, indicating highly crystallized structures. The XRD patters of the samples calcined at 1000 and 1100 ℃ showed that transition phases were still present, as evidenced by the characteristic peaks of ZnO at 2θ = 36.12°, 47.52°,62.86° and 67.96° [23]. When the temperature reached 1200 ℃, the pattern did not show any impurity phases compared to the standard data (ICSD card No. 16172). This suggests that the reaction among RH silica, $Zn(NO_3)_2$ ·$6H_2O$, and $Mn(NO_3)_2$ ·$4H_2O$ was completed, and the well-crystallized Zn_2SiO_4 with Mn^{2+} doped through its lattice was obtained at 1200 ℃ [23]. The appearances of the samples under visible light and 256 nm UV light excitation are shown in Figure 8, which showed that the color of the samples gradually changed from brown/grey to off-white. Based on rough visual inspection, all samples emitted green light, and a clear positive correlation between the emission intensity and the reaction temperature was observed. Considering single phase Zn_2SiO_4:0.08Mn^{2+} was successfully synthesized at 1200 ℃, higher temperature reaction conditions were not explored mainly out of the consideration of energy saving for potential future industrial production.

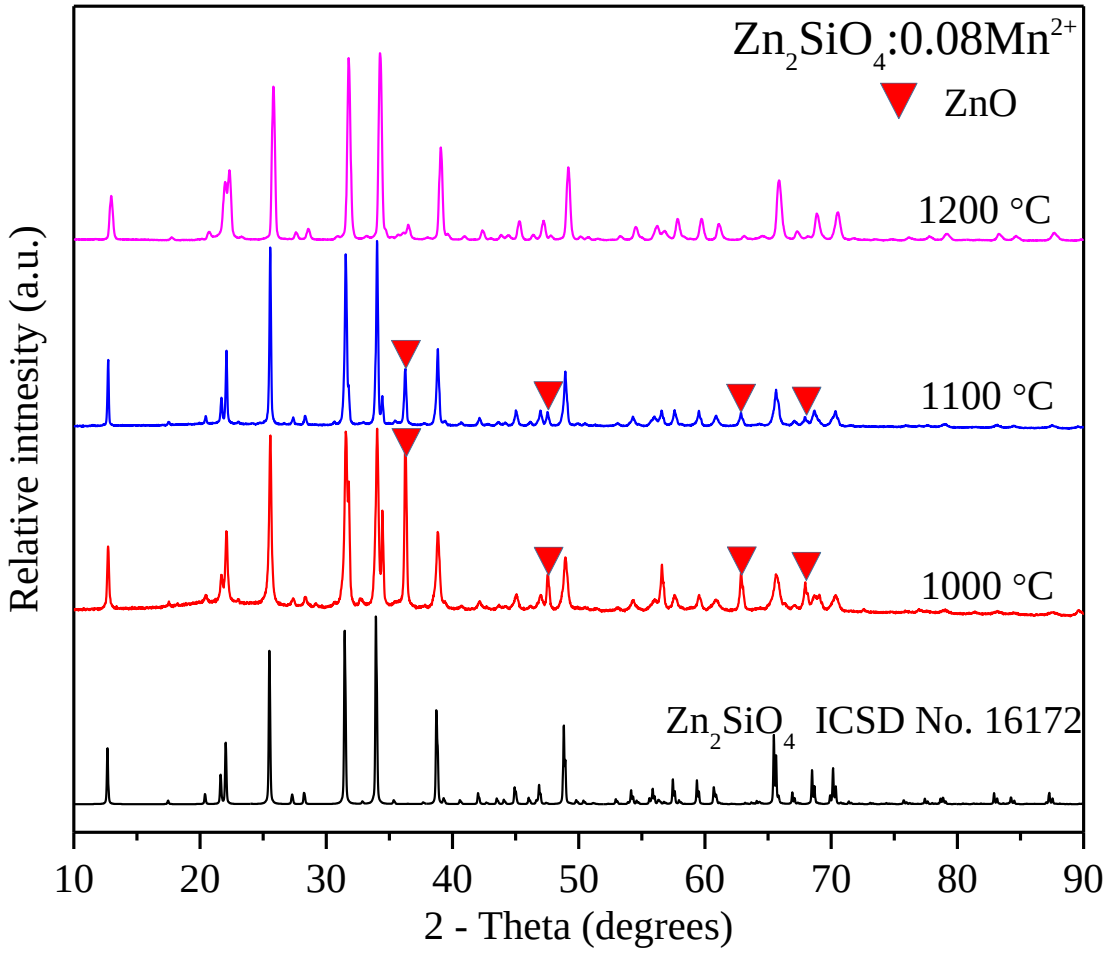

Figure 7. X-ray diffraction patterns of Zn_2SiO_4:0.08Mn^{2+} phosphors synthesized at temperatures of 1000, 1100, and 1200 ℃ under N_2 atmosphere for 4 hours.

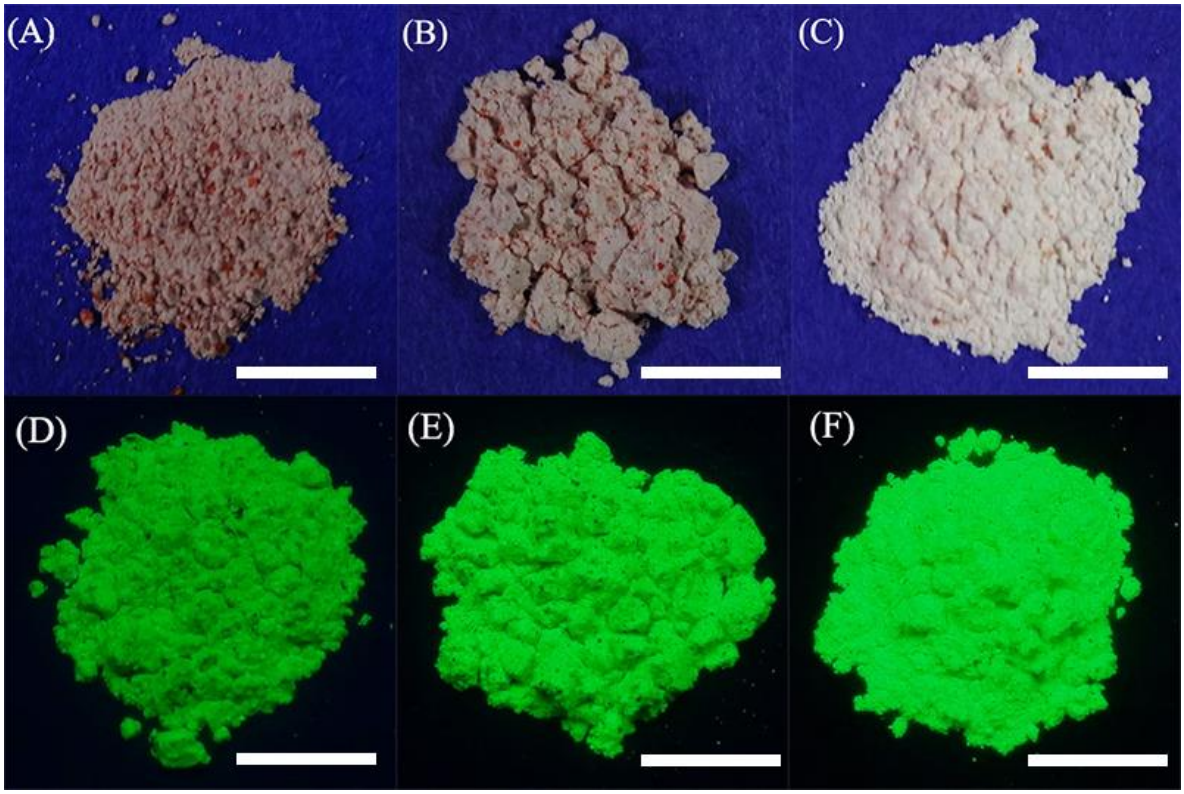

Figure 8. Appears of the RH phosphor samples prepared at different temperatures: 1000 ℃ (A and D), 1100 ℃ (B and E), and 1200 ℃ (C and F) under visible light (A-C) and 256 nm UV light (D-F). Scale bars represent 1 cm.

Figure 9a shows the PL spectra of the RH phosphor samples under 258 nm excitation. All the three PL spectra peaked at ca. 527 nm, corresponding to the electronic transition from $^4T_1$ to $^6A_1$ that limited the emission transition of Mn^{2+}. After excitation, the electrons returned to the ground state, and a green emission was observed [23a]. With an increasing reaction temperature, the PL intensity was improved significantly, well corresponding to the visual inspection under 254 nm UV light excitation as shown in Figure 4D-4F. The optimum PL intensity was achieved at a calcination temperature of 1200 ℃. According to Figure 9b, the quantum yield, which is the percentage of the excited electrons returned to the ground state, was improved with an increasing reaction temperature. Overall, the XRD patterns, visual inspection, PL intensity, and quantum

yields all indicate that a high reaction temperature of 1200 ℃ resulted in high quality phosphor derived from RH silica. Although sol-gel methods could better control the size of the phosphors, the high cost and the health and environmental issues associated with the sol-gel process are key drawbacks. The synthesis of phosphor derived using RH silica is appealing for sustainable development and is affordable.

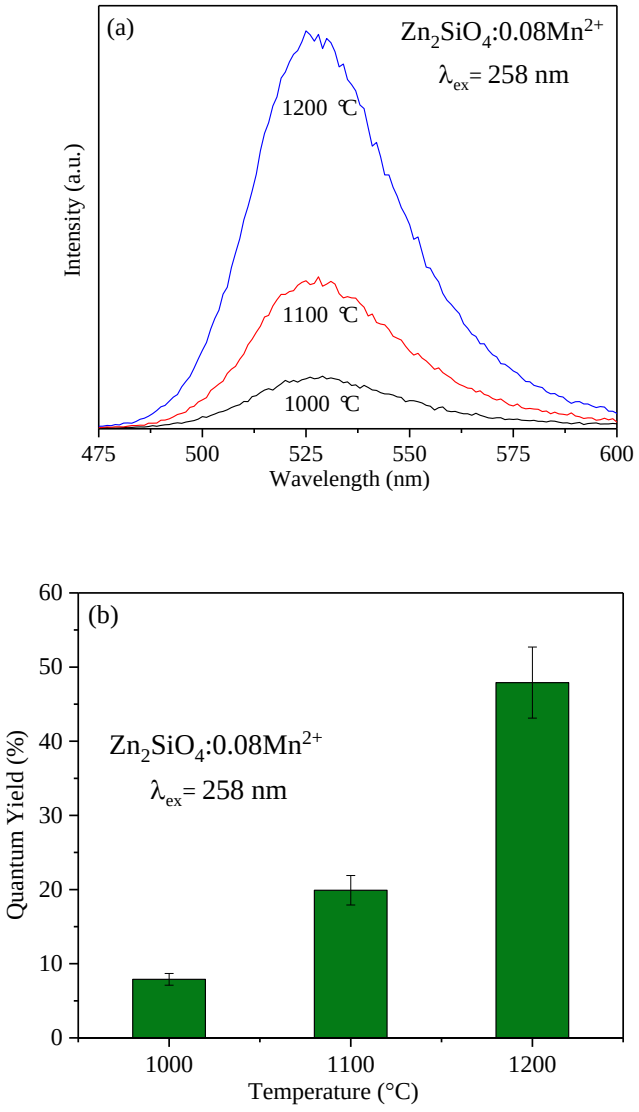

Figure 9. (a) PL spectra of the zinc silicate derived from the RH-silica under different temperatures. (b) The quantum yield variation of the samples corresponding to the PL spectra.

Composition is another key factor that influences the PL performance of silicate phosphors [24]. As such, the doping concentration in $Zn_2SiO_4:Mn^{2+}$, was adjusted to be 4%, 6%, 8%, 10%, 12% through the initial formulation. Based on the results above, all the samples were synthesized under the optimum reaction temperature of 1200 ℃ for 4 hours. The XRD patterns in Figure 10 indicate that all the samples doped with different concentrations of Mn could successfully form Zn_2SiO_4 single phase, as compared with the simulated pattern. This indicates that within certain range, doping concentration does not influence the formation of Zn_2SiO_4. All the samples are white powders, and they all emit high intensity green light under 258 nm UV light excitation. As expected, the PL emission intensity of the phosphors was affected by doping concentration. Figure 11a shows that the PL intensity of the doped phosphors was increased with an increasing Mn^{2+} doping concentration up to 6%, and then decreased with a further increase of Mn^{2+} doping concentration, probably due to the quenching concentration effect. It is resulted from the excited and unexcited activation interactions, leading to the excitation energy going down to the quenching sites [23a, 25]. According to Figure 11b, the quantum yield exhibited the same trend as the PL emission intensity. The broad PL spectra covered most of the visible light range, which is advantageous for such RH derived phosphors for various applications, such as LED lights, phosphor thermometry, toys, and lights for room decoration. To be noted, Figure 11 also shows that the $Zn_2SiO_4:0.06Mn^{2+}$ RH phosphor with concentration exhibited slightly higher PL intensity than $Zn_2SiO_4:0.08Mn^{2+}$, which was the concentration typically adopted by the commercial phosphors.

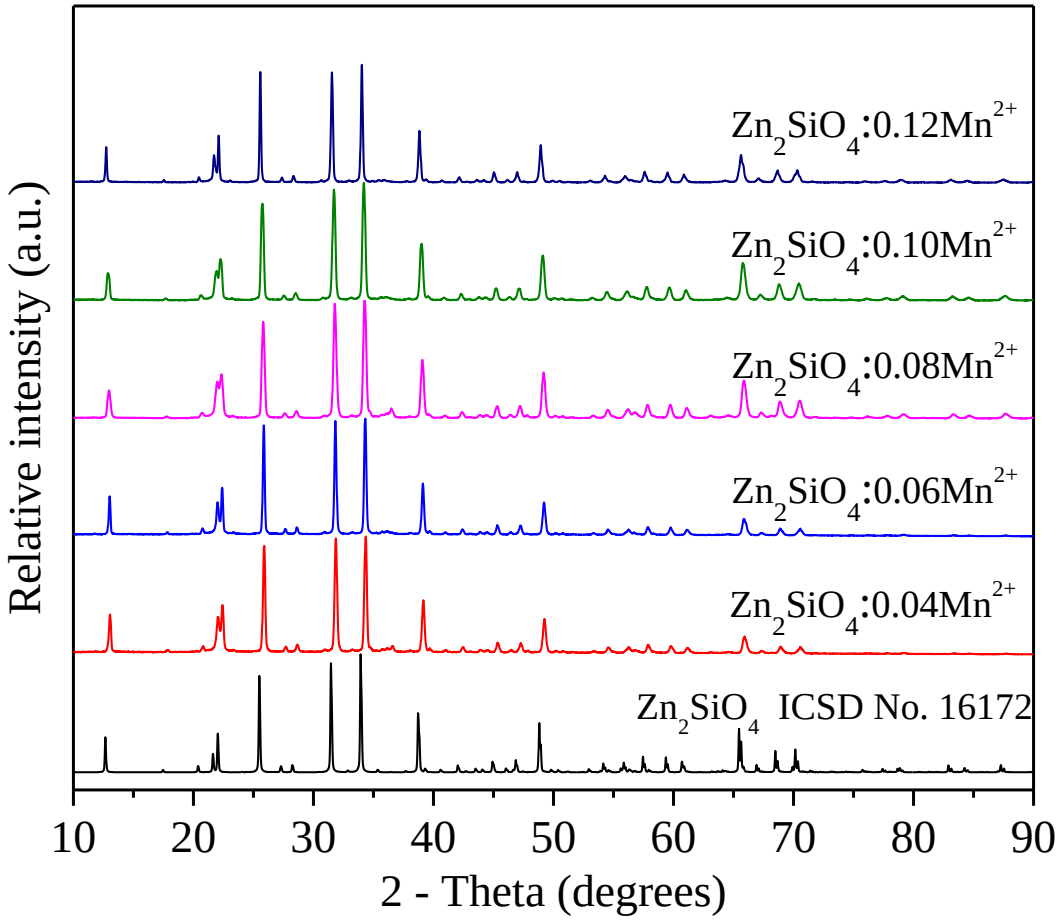

Figure 10. Powder X-ray diffraction patterns of the $Zn_2SiO_4:Mn^{2+}$ phosphors combustion-synthesized under different doping concentrations under 1200 ℃ for 4h.

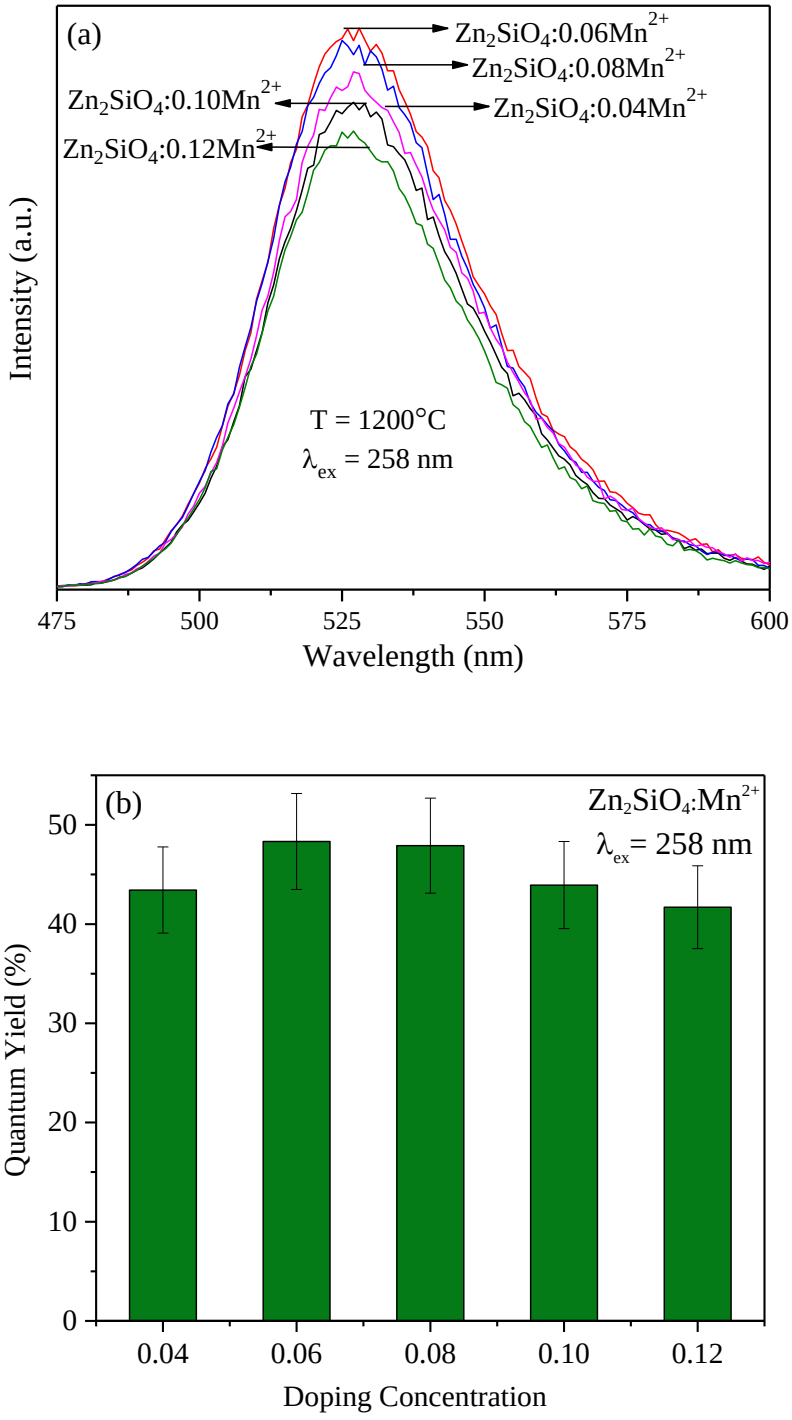

Figure 11. (a) PL spectra of the Zinc silicate derived from the RH-silica under different Mn2+ doped concentrations. (b) The quantum yield variation of the samples corresponding to the PL spectra.

Figure 12 shows the decay curve of Zn_2SiO_4:0.06Mn^{2+} sample excited by 258 nm to analyze the life time of the transition from $^4T_1$ to $^6A_1$. The curve fit a multi exponential function represented as

$$I(t) = A_1 e^{\left(-\frac{t}{\tau_1}\right)} + A_2 e^{\left(-\frac{t}{\tau_2}\right)},$$

where *t* represents time, τ_1 and τ_2 are two different fluorescence decay times, and A_1 and A_2 are the fit constants with values of 24 and 76, respectively [23a]. The fit of the kinetics for Zn_2SiO_4:0.06Mn^{2+}at 527 nm showed an average of 20 % contribution from the short (τ_1) component and 80 % contribution from the long (τ_2) component. The calculated lifetime values are τ_1 = 1.023 ms and τ_2 = 6.2 ms. The average decay time τ could be modeled with the equation below[26]:

$$\tau = \frac{A_1\tau_1^2 + A_2\tau_2^2}{A_1\tau_1 + A_2\tau_2}$$

(2)

Therefore, the average decay lifetime was 5.94 ± 0.12 ms. This value is shorter than the reported data ranges of 8-16 ms [27], which is advantageous for applications such as PDP.

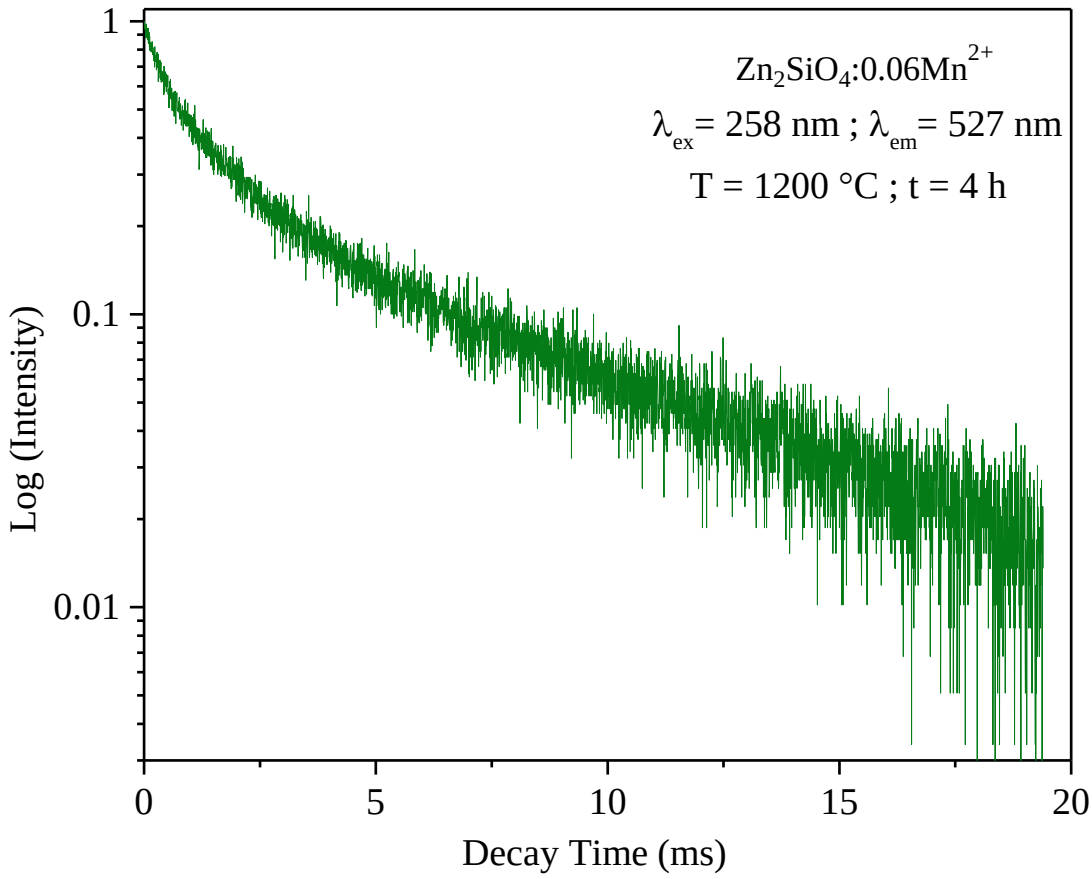

Figure 12. Decay curve of the green emission at 527 nm under 258 excitation from the $Zn_2SiO_4:0.06Mn^{2+}$ phosphor.

The high price of commercial phosphors is the main disadvantage for their applications in industry. RH silica could be an appealing alternative to significantly lower the price of phosphors for wider applications. To insure quality, control silicate phosphor samples were synthesized under N_2 atmosphere at 1200 ℃ for 4 hours from silicic acid [19] and commercial silica [20], which were used in the production of commercial phosphors, with the same doping concentration $Zn_2SiO_4:0.08Mn^{2+}$ [23a] for comparison. All samples were white powders and emitted highly intensive green light, hard to be differentiated by the naked eyes. Figure 13a shows the PL excitation spectra of the phosphors derived from commercial silica, RH silica, and silicic acid. The

results showed that the phosphor from commercial silica exhibited the lowest intensity and the one derived from silicic acid exhibited the highest intensity under 258 nm excitation. The quantum yield of the samples followed the same trend as their PL intensity, as shown in Figure 13b. These results showed that RH phosphor exhibited PL performance than the phosphor from commercial silica. This is probably due to the high specific surface area of RH silica, which contributes to a large interface between the reactants, reducing the diffusion distance between silica and metal nitrates, leading to improved reaction kinetics between the silica and metal nitrates. The phosphor from the silicic acid exhibited the best PL performance. However, silicic acid is not an appealing material to synthesize phosphors due to its high cost. Although the RH biomass phosphor did not outperform silicic acid, it still reached 70% efficiency of the phosphor from silicic acid. Considering preparing silica from RHs is cost effective and energy efficient, and the PL property is better than the phosphor from the commercial silica, therefore RH phosphor represents a viable alternative, which could be beneficial for applications in industries.

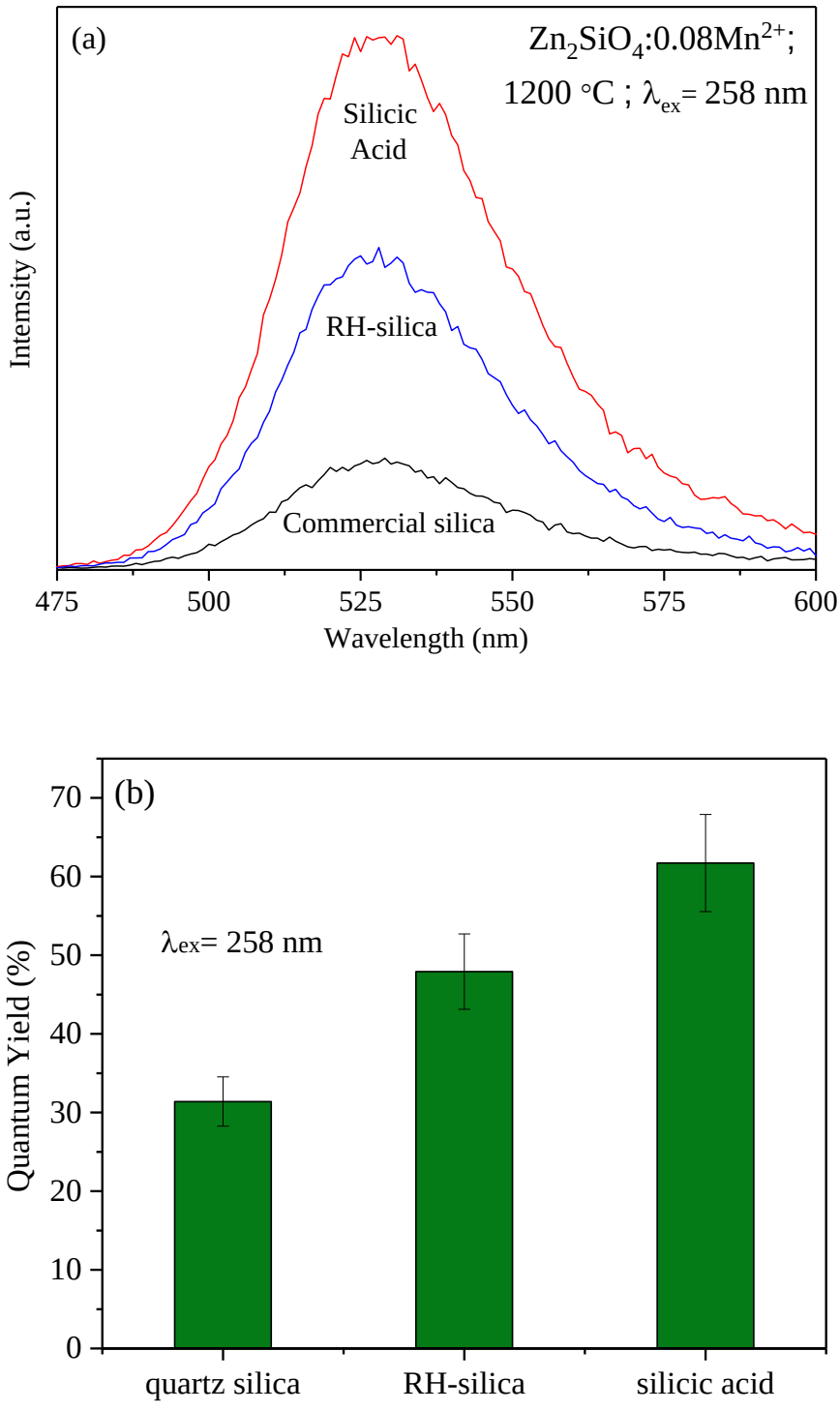

Figure 13. (a) PL spectra of the zinc silicate derived from the RH-silica, commercially-used silica, and silicic acid. (b) The quantum yield variation of the sample corresponding to the PL spectra.

2.4 Conclusion

In summary, amorphous silica was extracted from acid-treated RH biomass by using the direct calcination method. After mixing RH-silica, Zn^{2+}, and Mn^{2+} related metal salts, $Zn_2SiO_4:Mn^{2+}$ green phosphor was obtained via high temperature pyrolysis. By controlling the temperature and Mn^{2+} doping concentration, the optimum reaction conditions were found. Under such conditions, the sample of $Zn_2SiO_4:0.08Mn^{2+}$ after treatment at 1200 ℃ for 4 hours was obtained. Compared to the sample made from silicic acid and commercially-used silica, PL intensity and quantum yield of the RH silicate phosphor was better than the sample derived from commercially-used silica and reached 70 % efficiency of the sample made from silicic acid. The results showed that the phosphor derived from RH can serve as an alternative to commercially-used phosphor due to its favorable properties and inexpensive green resource.

References

1. (a) Soltani, N.; Bahrami, A.; Pech-Canul, M.; González, L., Review on the physicochemical treatments of rice husk for production of advanced materials. *Chemical engineering journal* **2015,** *264*, 899-935; (b) Pode, R., Potential applications of rice husk ash waste from rice husk biomass power plant. *Renewable and Sustainable Energy Reviews* **2016,** *53*, 1468-1485.
2. Gadde, B.; Bonnet, S.; Menke, C.; Garivait, S., Air pollutant emissions from rice straw open field burning in India, Thailand and the Philippines. *Environmental Pollution* **2009,** *157* (5), 1554-1558.
3. Chen, H.; Wang, W.; Martin, J. C.; Oliphant, A. J.; Doerr, P. A.; Xu, J. F.; DeBorn, K. M.; Chen, C.; Sun, L., Extraction of lignocellulose and synthesis of porous silica nanoparticles from rice husks: a comprehensive utilization of rice husk biomass. *ACS Sustainable Chemistry & Engineering* **2012,** *1* (2), 254-259.
4. Saha, B. C.; Cotta, M. A., Lime pretreatment, enzymatic saccharification and fermentation of rice hulls to ethanol. *Biomass and Bioenergy* **2008,** *32* (10), 971-977.
5. (a) Li, Y.; Lan, J. Y.; Liu, J.; Yu, J.; Luo, Z.; Wang, W.; Sun, L., Synthesis of Gold Nanoparticles on Rice Husk Silica for Catalysis Applications. *Industrial & Engineering Chemistry Research* **2015,** *54* (21), 5656-5663; (b) Artkla, S.; Kim, W.; Choi, W.; Wittayakun, J., Highly enhanced photocatalytic degradation of tetramethylammonium on the hybrid catalyst of titania and MCM-41 obtained from rice husk silica. *Applied Catalysis B: Environmental* **2009,** *91* (1), 157-164.
6. Adam, F.; Chua, J.-H., The adsorption of palmytic acid on rice husk ash chemically modified with Al (III) ion using the sol–gel technique. *Journal of colloid and interface science* **2004,** *280* (1), 55-61.
7. Wang, W.; Martin, J. C.; Huang, R.; Huang, W.; Liu, A.; Han, A.; Sun, L., Synthesis of silicon complexes from rice husk derived silica nanoparticles. *RSC Advances* **2012,** *2* (24), 9036-9041.
8. (a) Wang, W.; Martin, J. C.; Fan, X.; Han, A.; Luo, Z.; Sun, L., Silica nanoparticles and frameworks from rice husk biomass. *ACS applied materials & interfaces* **2012,** *4* (2), 977-981; (b) Wang, W.; Martin, J. C.; Zhang, N.; Ma, C.; Han, A.; Sun, L., Harvesting silica nanoparticles from rice husks. *Journal of Nanoparticle Research* **2011,** *13* (12), 6981-6990.
9. Sun, L.; Gong, K., Silicon-Based Materials from Rice Husks and Their Applications. *Industrial & Engineering Chemistry Research* **2001,** *40* (25), 5861-5877.
10. Pineda-Vásquez, T. G.; Casas-Botero, A. E.; Ramírez-Carmona, M. E.; Torres-Taborda, M. M.; Soares, C. H.; Hotza, D., Biogeneration of Silica Nanoparticles from Rice Husk Ash Using Fusarium oxysporum in Two Different Growth Media. *Industrial & Engineering Chemistry Research* **2014,** *53* (17), 6959-6965.
11. Wang, Z.; Chen, H.; Xu, L.; Xu, S. Q.; Gao, C. F.; Oliphant, A. J.; Liu, J.; Lu, Y.; Wang, W.; Sun, L., Synthesis and colour prediction of stable pigments from rice husk biomass. *Green Materials* **2015,** *3* (1), 10-14.
12. Roschat, W.; Siritanon, T.; Yoosuk, B.; Promarak, V., Rice husk-derived sodium silicate as a highly efficient and low-cost basic heterogeneous catalyst for biodiesel production. *Energy Conversion and Management* **2016,** *119*, 453-462.

13. Fernandes, G. P.; Yadav, G. D., Atom-Economical Selective-Ring-Opening Reaction of Glycidol with 1-Naphthol Catalyzed by Magnesium Silicate of a Biogenic Silica Source. *Industrial & Engineering Chemistry Research* **2015,** *54* (42), 10245-10252.
14. Lojpur, V.; Nikolić, M.; Jovanović, D.; Medić, M.; Antić, Ž.; Dramićanin, M., Luminescence thermometry with Zn2SiO4: Mn2+ powder. *Applied Physics Letters* **2013,** *103* (14), 141912.
15. Wang, L.; Liu, X.; Hou, Z.; Li, C.; Yang, P.; Cheng, Z.; Lian, H.; Lin, J., Electrospinning synthesis and luminescence properties of one-dimensional Zn_2SiO_4: Mn^{2+} microfibers and microbelts. *The Journal of Physical Chemistry C* **2008,** *112* (48), 18882-18888.
16. Wang, Y.; Hao, Y.; Yuwen, L., Synthesis process dependent photoluminescent properties of Zn_2SiO_4: Mn^{2+} upon VUV region. *Journal of alloys and compounds* **2006,** *425* (1), 339-342.
17. Yu, X.; Wang, Y., Synthesis and VUV spectral properties of nanoscaled Zn 2 SiO 4: Mn 2+ green phosphor. *Journal of Physics and Chemistry of Solids* **2009,** *70* (8), 1146-1149.
18. Lukić, S.; Petrović, D.; Dramićanin, M.; Mitrić, M.; Đačanin, L., Optical and structural properties of Zn_2SiO_4: Mn^{2+} green phosphor nanoparticles obtained by a polymer-assisted sol–gel method. *Scripta Materialia* **2008,** *58* (8), 655-658.
19. Kasenga, A. F.; Gray, L. F.; Henson, T. L.; Macinnis, M. B., Method for a producing manganese activated zinc silicate phosphor. Google Patents: 1990.
20. (a) King, E., Heats of Formation of Crystalline Calcium Orthosilicate, Tricalcium Silicate and Zinc Orthosilicate1. *Journal of the American Chemical Society* **1951,** *73* (2), 656-658; (b) Takesue, M.; Hayashi, H.; Smith, R. L., Thermal and chemical methods for producing zinc silicate (willemite): a review. *Progress in Crystal Growth and Characterization of Materials* **2009,** *55* (3), 98-124.
21. (a) Pokhrel, M.; Wahid, K.; Mao, Y., Systematic Studies on RE2Hf2O7: 5% Eu^{3+} (RE= Y, La, Pr, Gd, Er, and Lu) Nanoparticles: Effects of the A-Site RE^{3+} Cation and Calcination on Structure and Photoluminescence. *The Journal of Physical Chemistry C* **2016**; (b) Pokhrel, M.; Kumar, G.; Ma, C.-G.; Brik, M.; Langloss, B. W.; Stanton, I. N.; Therien, M. J.; Sardar, D.; Mao, Y., Electronic and optical properties of Er-doped Y_2O_2S phosphors. *Journal of Materials Chemistry C* **2015,** *3* (43), 11486-11496.
22. (a) Liu, J.; Wang, Y.; Yu, X.; Li, J., Enhanced photoluminescence properties of Zn_2SiO_4: Mn^{2+} co-activated with Y^{3+}/Li^+ under VUV excitation. *Journal of Luminescence* **2010,** *130* (11), 2171-2174; (b) Morell, A.; El Khiati, N., Green phosphors for large plasma TV screens. *Journal of The Electrochemical Society* **1993,** *140* (7), 2019-2022.
23. (a) Lu, Q.; Wang, P.; Li, J., Structure and luminescence properties of Mn-doped Zn 2 SiO 4 prepared with extracted mesoporous silica. *Materials Research Bulletin* **2011,** *46* (6), 791-795; (b) Li, Z.; Zhang, H.; Fu, H., Facile synthesis and morphology control of Zn_2SiO_4:Mn nanophosphors using mesoporous silica nanoparticles as templates. *Journal of Luminescence* **2013,** *135*, 79-83.
24. (a) Alaparthi, S. B.; Lu, L.; Tian, Y.; Mao, Y., Europium doped lanthanum zirconate nanoparticles with high concentration quenching. *Materials Research Bulletin* **2014,** *49*, 114-118; (b) Pokhrel, M.; Valdes, C.; Mao, Y., Ultraviolet upconversion enhancement in triply doped $NaYF_4$: Tm^{3+}, Yb^{3+} particles: The role of Nd^{3+} or Gd^{3+} Co-doping. *Optical Materials* **2016,** *58*, 67-75.
25. (a) Thiyagarajan, P.; Kottaisamy, M.; Rao, M. R., Structural and luminescence properties of pulsed laser deposited green-emitting Zn_2SiO_4: Mn phosphor thin films. *Scripta materialia* **2007,** *57* (5), 433-436; (b) Kang, Z.; Liu, Y.; Wagner, B.; Gilstrap, R.; Liu, M.; Summers, C.,

Luminescence properties of Mn^{2+} doped Zn_2SiO_4 phosphor films synthesized by combustion CVD. *Journal of luminescence* **2006,** *121* (2), 595-600.
26. Fujii, T.; Kodaira, K.; Kawauchi, O.; Tanaka, N.; Yamashita, H.; Anpo, M., Photochromic behavior in the fluorescence spectra of 9-anthrol encapsulated in Si-Al glasses prepared by the sol-gel method. *The Journal of Physical Chemistry B* **1997,** *101* (50), 10631-10637.
27. Rao, R.; Devine, D., RE-activated lanthanide phosphate phosphors for PDP applications. *Journal of Luminescence* **2000,** *87*, 1260-1263.

Chapter 3. Self-Assembled Multifunctional Lignocellulose Aerogel and Silica Nanoparticles from Rice Husks: a Comprehensive Utilization Strategy

3.1 Introduction

Rice husks (RHs) are one of the most abundant sources of biomass in the world, due to the massive amount of rice consumption by human population. There are two main components in RHs: silica (ca.15-28 wt. %) and lignocellulose (LC) (ca.72-85 wt. %) [1]. If isolated, the silica from RHs could be used to prepare various silicon-based materials, including silicon carbide [2], silicon nitride [3], silicon tetrachloride [4], silicon [5], and zeolite [6]. These materials have widespread application in semiconductor materials [6], abrasive materials [6], pigments [7], catalyst supports [8], etc. LC is a complex of organic materials, which includes lignin, cellulose, and hemicellulose [9]. LC could be considered as a resource for various biochemicals, such as bioethanol and xylitol [10]. One of the three major contents of LC, cellulose, is abundantly available in nature, and it has been used by humans for a wide range of applications, such as paper goods, for thousands of years. Recently, cellulose has found applications across several areas of study, including cellulose gas barrier films [11], sensors [12], cellulose nanocrystals [12], and aerogels [13]. However, the extraction process of RH cellulose is very complex and time consuming [14]. Ionic liquids (ILs) were reported to be able to effectively dissolve cellulose and lignin [15]. The method utilizes the ions in ILs as the acceptor of hydrogen bonds [16]. The hydrogen bonds could separate cellulose molecules from other polysaccharides in biomass, making cellulose dissolved in ILs [17]. As such, ILs are a good working medium to directly extract the organic components from RH biomass, and dissolve those organic contents to form a homogeneous system.

Aerogels are a group of materials with a 3-D porous network structure. Their ultra-low density, high surface area, and large porosity make them attractive for many applications, including

catalysts [18], artificial muscles [19], supercapacitors [20], and absorption materials [21]. Carbon aerogels are extremely promising due to their low density, high conductivity, high porosity, and large surface area. Graphene and carbon nanotubes from chemical vapor deposition (CVD), and resorcinol-formaldehyde aerogels derived from pyrolysis are the three main resources to prepare carbon aerogels [22]. However, the precursors are very expensive, and some of the chemicals used are also unfriendly to environment.

ILs were reported to effectively dissolve LC from RHs [9, 17]. By using a liquid nitrogen free-thaw (NFT) process [23], subsequent water regeneration, and CO_2 supercritical drying, self-assembled LC aerogels can be prepared [17, 23a]. Their high porosity and surface area allow the LC aerogels, particularly after some surface modification, to be ideal absorption materials for various applications such as oil spill treatment. Carbon aerogels can be further obtained via high temperature pyrolysis of LC aerogels under inert gas. The porous structure could be maintained and the entire organic components could be completely converted into carbon. Their remarkable chemical and physical properties make carbon aerogels promising for various applications, such as supercapacitors [24], catalyst supports [25], and gas storage [25b].

With an aim to achieve a comprehensive application of RH biomass, it is designed to first dissolve the LC in RHs using IL. Subsequently, the undissolved RH residue with a high concentration of silica was thermally treated to synthesize silica nanoparticles. Brief examples of potential applications of the self-assembled LC aerogel and silica nanoparticles are presented.

3.2 Experimental

3.2.1 Materials

RHs (obtained from Rice Hull Specialty Products, Inc., Stuttgart, AR) were washed by diluted hydrochloric acid (35%, Fisher Scientific) and ground into powders. 1-Butyl-3-

methylimidazolium chloride (BMIMCl, ≥95%, BASF) was used for dissolving the LC in RHs. Acetone (99.9%, Sigma-Aldrich) was used for the CO_2 supercritical drying unit.

3.2.2 Preparation of LC aerogel

The HCl treated RHs were dried overnight in an oven at 80 ℃ to eliminate moisture. Then, the dried RH sample was mixed with BMIMCl at a mass ratio of 1:12 and the mixture was maintained at 85 ℃ for 4 hours. The mixture was then centrifuged at 32,200 g force for 20 minutes to separate the undissolved RH residue, which was stored for further use. The homogeneous BMIMCl solution containing LC was frozen with liquid nitrogen (-196 ℃) for 6 hours. Then the frozen sample was placed in a vacuum oven to slowly thaw under room temperature (25 ℃) for 6 hours. The NFT process was repeated 5 times. The treated sample was then rinsed in DI water to remove BMIMCl. The DI water was tested in the replenish process until the Cl^- residue cannot be detected by $AgNO_3$.

The LC hydrogel sample was then treated in acetone for 3 days to exchange water with acetone. After that, the sample was transferred into a CO_2 supercritical drying unit and mixed with acetone. Subsequently, liquid carbon dioxide was charged to the autoclave, and the system was purged. The white CO_2/acetone mixture was periodically collected for testing until the acetone was completely exchanged with CO_2. A multiple-stage drying process was then conducted from -20 ℃ to 42 ℃, and the final pressure was 1300 psi. The slow depressurization process was completed ca. 3 to 6 hours to insure no cracks on the aerogel samples. Finally, the self-assembled LC aerogel was prepared.

In order to compare the structure of the regenerated lignocellulose aerogel with the pristine cellulose, RH cellulose was also prepared [26]. RHs were rinsed with water at 70 °C for 4 hours, then filtered and dried at 60 °C in an oven. The dried RHs were then treated with 5.0 wt. % NaOH

solution (1:20 mass ratio) at room temperature for 2 hours under vigorous stirring. During the base treatment, majority of silica, lignin, and hemicellulose were dissolved in NaOH, the remaining cellulose was obtained by filtration [26]. The obtained cellulose was then bleached by a buffer solution prepared by mixing 24.0 wt. % H_2O_2 and 4.0 wt. % NaOH at 1:1 mass ratio at 45 ℃ for 2 hours. The mass ratio of the cellulose and the buffer solution was 1:20. The bleaching process was repeated for 4 times. After drying the sample at 60 ℃, RH cellulose was obtained.

3.2.3 Hydrophobic modification of RH LC aerogel

The prepared RH LC aerogel (ca. 0.19 g) was treated with methyltrimethoxysilane (MTMS, 300 μL) vapor in a glass container at 70 °C for 2 hours. Afterwards, the unreacted MTMS was removed by evacuating the container. This method was designed to avoid direct contact between RH-LC aerogel and liquid MTMS, which may potentially damage the original network structure of the aerogel.

3.2.4 Preparation of carbon aerogels

Carbon aerogels were prepared via the pyrolysis of the LC aerogel in a tube furnace (MTI OTF1200X) under nitrogen atmosphere at a conditioning temperature of 1000 ℃ for 2 hours. The furnace was heated up to the setting temperature with a heating rate of 5 ℃/min. The tube was purged with N_2 for 4 hours prior to pyrolysis and the nitrogen flow rate was maintained at 200 cm^3/min during the entire pyrolysis process. The carbon aerogel was obtained when furnace was cooled to room temperature.

3.2.5 Preparation of RH silica nanoparticles

The RH residue after BMIMCl extraction was washed with DI water 5 times to remove the BMIMCl. Then the sample was dried in an oven at 80 ℃ for 24 hours. The dried RH residue was calcined at 700 ℃ in an air atmosphere for 2 hours to synthesize silica nanoparticles [9].

3.2.6 Characterization

The self-assembled LC aerogel and carbon aerogel 3-D porous network structures was characterized by a field emission scanning electron microscope (FE-SEM) (FEI Helios, Nanolab G3, Dual-Beam FIB/SEM). X-ray diffraction (XRD) patterns of the LC aerogel and carbon aerogel were recorded on an X-ray diffractometer (Bruker D5005, 40 kV and 40 mA, Cu K_α radiation (λ = 0.1540 nm). The N_2 adsorption and desorption curves, Brunauer-Emmet-Teller (BET) surface areas measured by a surface area and porosity analyzer (Nova 2000e, Quantachrome Instruments).

Water contact angles of the samples were measured on a Pedant Drop Tensiometer (OCA 20, Future Digital Scientific Corp., USA) to evaluate the hydrophobic properties of the MTMS treated LC aerogel. In the test, 0.5 μL water drops were controlled by a syringe system and dispensed drop by drop on the sample surface.

3.3 Results & Discussion

3.3.1 Formation of LC aerogel from RHs

Figure 14 shows the flow chart of the entire process for preparing self-assembled LC aerogel, carbon aerogel, and silica nanoparticles. RHs were first treated by BMIMCl at 85 ℃ for 4 hours. The obtained mixture was separated by centrifuge. The supernatant after centrifuge was collected and underwent an NFT process for 5 cycles to obtain LC freeze gel. Then the sample was washed with DI water to remove IL. Acetone solvent exchange was carried out subsequently for CO_2 supercritical drying. After drying, the self-assembled LC aerogel was obtained. The prepared LC aerogel was further pyrolyzed under N_2 atmosphere at 1000 ℃ to prepare carbon aerogel.

The RH residue obtained after centrifuging was cleaned by DI water and dried in an oven for 24 hours. Amorphous silica nanoparticles were prepared by calcining the RH residue at 700 °C for 2 hours under an air atmosphere.

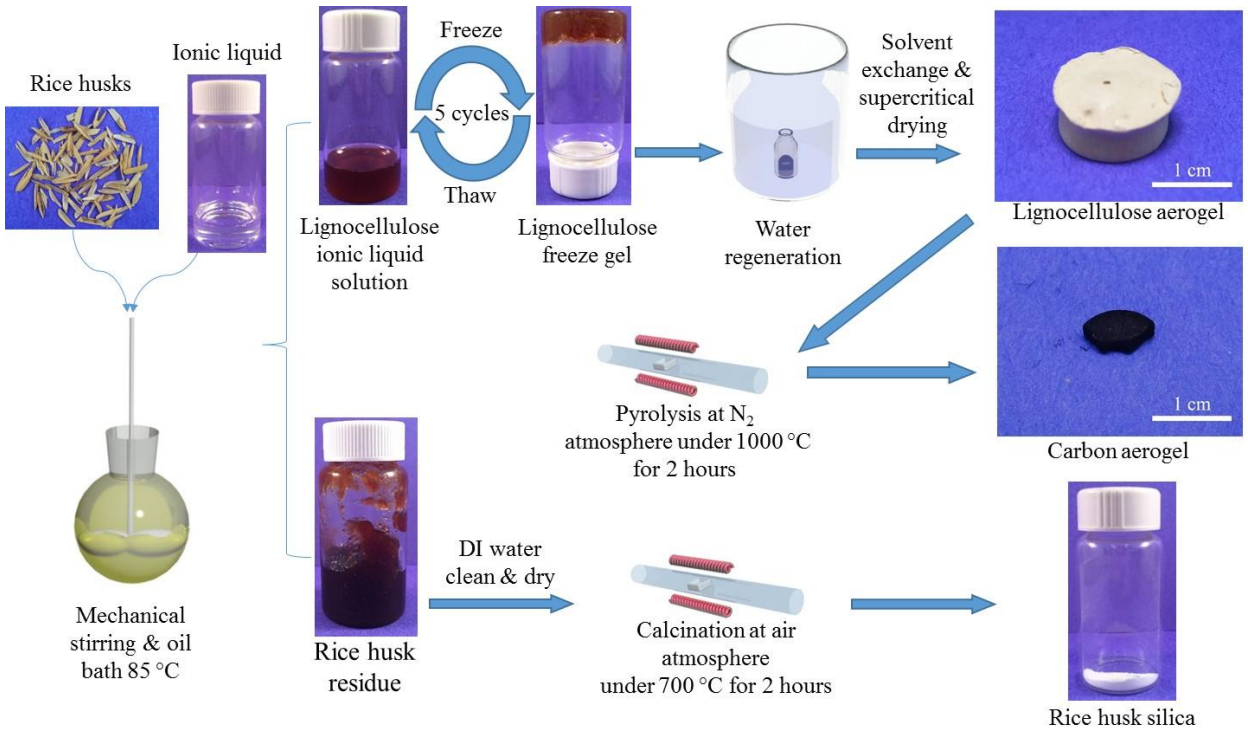

Figure 14. Flow chart of the process to prepare LC aerogel, carbon aerogel, and RH silica.

RHs, which contain a high content of LC, were partially dissolved in BMIMCl after 4 hours of treatment at 85 ℃ [9, 16]. The obtained LC IL solution was obtained after centrifugation and subsequently treated by the NFT process to induce gelation [17, 23b]. First, the LC solution in IL was frozen by liquid nitrogen, during which the IL solvent began to freeze so that it contained the frozen phase and the unfrozen liquid micro-phase [23b]. After being frozen for ca. 6 hours, cellulose, hemicellulose, and lignin were extruded by the completely frozen IL crystalline. In this process, the gap between cellulose macromolecules shrunk. The molecules were then crosslinked by physically twisted crosslinking points [23b]. Finally, a gel formed during a slow thawing process. This was due to an increasing strength of the physical crosslinking points with an increasing temperature. By utilizing CO_2 supercritical drying, a light LC aerogel was obtained. As shown in Figure 15, the self-assembled LC aerogel was light enough to stand on a dandelion. The density of the LC aerogel was measured to be 0.129 g/cm^3. This approach to prepare light aerogel is

advantageous because of three reasons. First, the formation process does not use any crosslinking agent, which may cause environmental and health issues. Second, the process is very facile and easy to scale up. The self-assembled thermodynamic process minimizes the utilization of chemicals. Third, eco-friendly RHs were used as the staring materials.

Figure 15. Digital picture of a lignocellulose aerogel on a dandelion.

The cross section of the LC aerogel derived from RHs were characterized by SEM and the images are presented in Figure 16, which show that the LC IL solution formed a steady network structure with a dense porosity. The higher resolution SEM image indicates that the LC fibers interconnected at physical crosslinking points [17, 23b]. The result suggested that the cycled water regeneration could effectively remove IL, eliminating the barrier of the following gelation process. Overall, the NFT process could successfully lead to the formation of hydrogel from the IL LC solution. With the assistance of CO_2 supercritical drying, the hydrogel could maintain its porous network structure, promising for a wide variety of applications related to porous materials [23b].

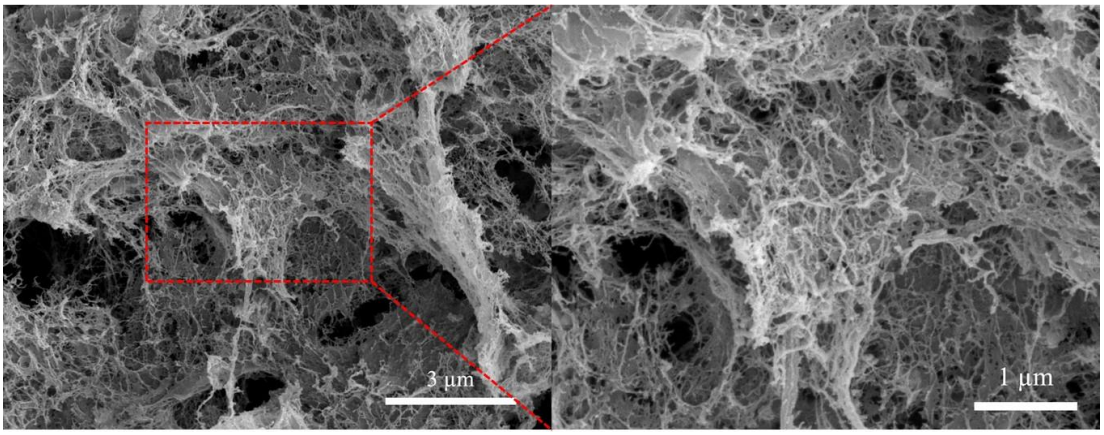

Figure 16. SEM images of the LC aerogel synthesized after 5 cycles of NFT.

3.3.2 Formation of carbon aerogel

Self-assembled LC aerogel is a porous material that contains a lot of element C. Thus, carbon aerogel could be generated from LC aerogel in inert gas atmosphere under elevated temperatures. As shown in Figure 17, the porous network structure was well maintained throughout the high temperature pyrolysis, which indicates that LC aerogel could maintain its structure at elevated temperatures. The inert gas atmosphere also contributed to minimizing the damage of the porous structure. The lignin and hemicellulose wrapped around cellulose changed to spheres after pyrolysis, attached to the carbonized cellulose structure [27].

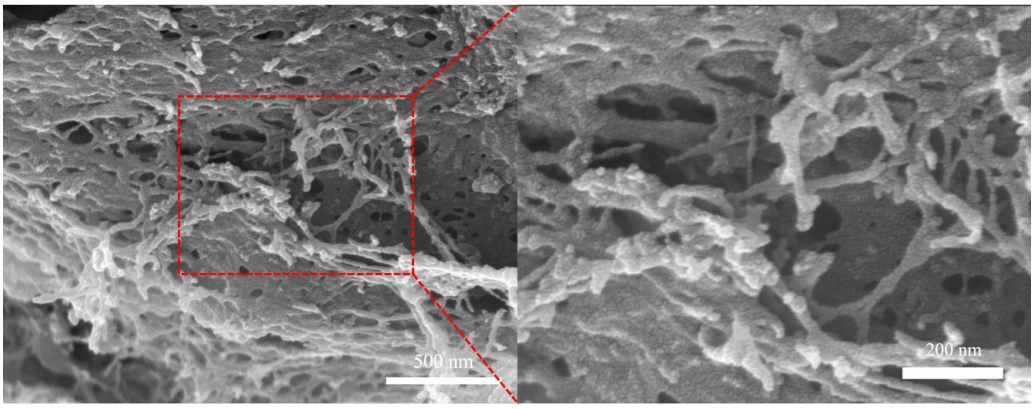

Figure 17. SEM images of the carbon aerogel prepared via the pyrolysis of LC aerogel under 1000 ℃ for 2 hours.

Figure 18 shows the XRD patterns of the LC aerogel, RH cellulose, and carbon aerogels. The results show that RH cellulose bears the typical cellulose I structure according to the characteristic peaks (002), (101), and (040) at 15.5 °, 22.1 °, and 34.7 °, respectively [28]. The LC aerogel was obtained after water regeneration and CO_2 supercritical drying. It mainly showed one broad hump at ca. 21.1 °, which indicates that the regenerated LC has a lower level of crystallinity than the raw cellulose, which is expected [29]. According to the previous reports [30], the regenerated cellulose or lignocellulose possess a cellulose II structure with a characteristic peak (002) at 12.1 °, which is also shown in the XRD pattern of LC aerogel. The lowered crystallinity of the regenerated LC is because some of the intrinsic inter- and intra-molecular hydrogen bonds and crystallized structures of cellulose was destroyed in the dissolving process [29]. However, the intensity of peak (002) of the LC aerogel is relatively low as shown in Figure 5a. This is likely due to the fact that lignin restrained the swelling of cellulose molecules in IL and limited the solubility of cellulose molecules at relatively low temperatures (85 ℃) [23b, 30b, 31].

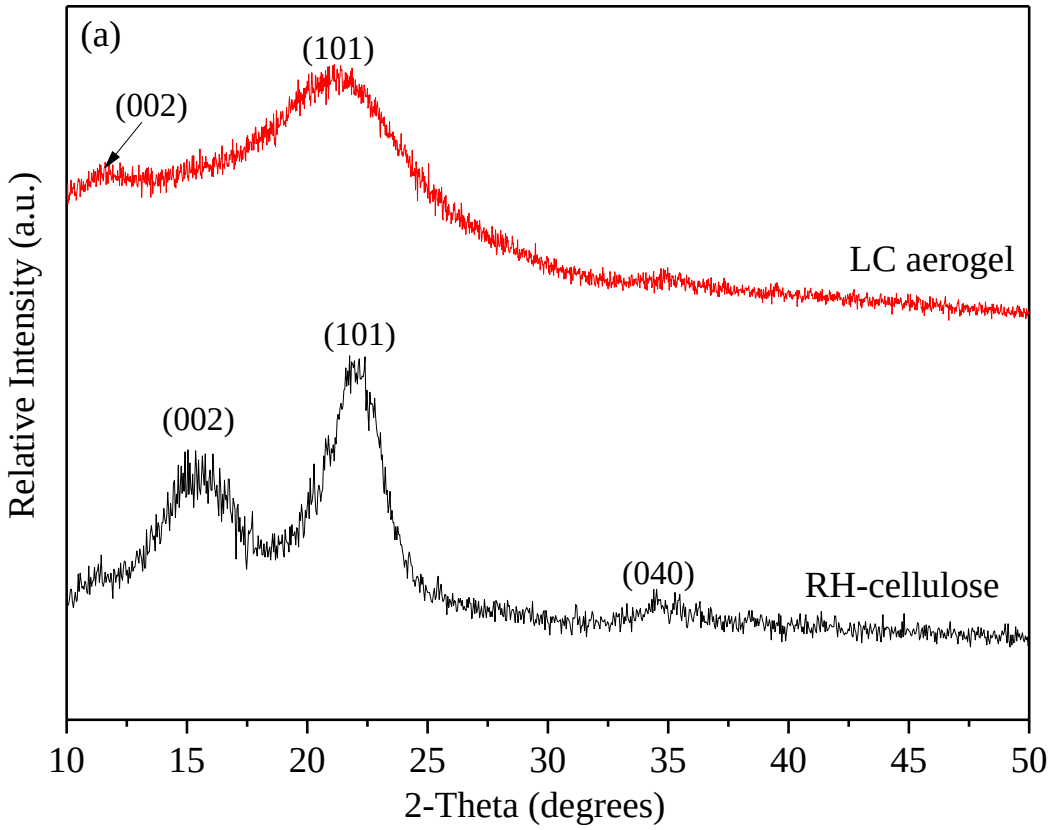

Figure 18. XRD patterns of the LC aerogel and the cellulose derived from RHs

3.3.3 Porosity properties and surface areas of the LC aerogel and carbon aerogels

As shown in Figure 19, the N_2 adsorption-desorption curves of the LC aerogel and carbon aerogel prepared at 1000 °C are of type IV, suggesting that the two types of aerogels are mesoporous. The curves also indicate that the LC aerogel formed a mesoporous network structure after cycled NFT thermodynamic crosslinking, and the carbon aerogel maintained a porous structure after pyrolysis. Based on the isotherms, the specific surface area (SSA) and pore property data were calculated and are summarized in Table 3. The LC aerogel derived from RHs has a relatively higher total specific surface area ($SSA_{(total)}$) of 106.5 m^2/g, compared to the literature data of 80.7 m^2/g [17]. The main reason is probably because RHs contain a high cellulose content [32], which could minimize the effect of lignin in the solution and assist the formation of a porous

network structure. The LC aerogel also has a high SSA $_{(meso)}$/SSA $_{(total)}$ ratio, which is probably owing to the low surface tension at the supercritical CO_2/hydrogel interface during CO_2 supercritical drying. After the conversion of LC aerogel to carbon aerogel, the SSA $_{(total)}$ of the carbon aerogel sample increased from 106.5 to 217.3 m^2/g after pyrolysis.

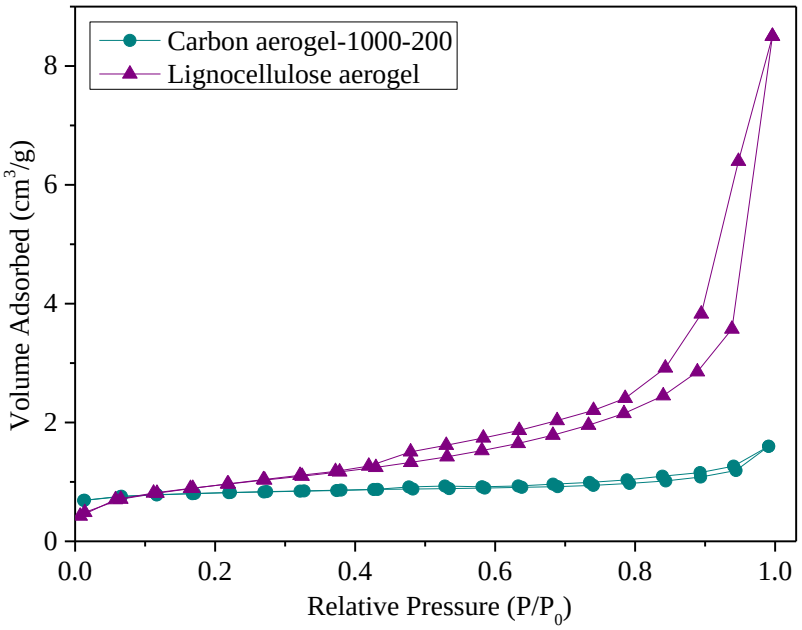

Figure 19. N_2 adsorption-desorption isotherms of the LC aerogel and carbon aerogel.

Table 3. Surface area of the LC aerogel and carbon aerogel.

Sample	$SSA_{(total)}$ [m^2/g]	$SSA_{(meso)}$ [m^2/g]	$SSA_{(micro)}$ [m^2/g]	$SSA_{(meso)}/SSA_{(total)}$ [%]	$SSA_{(micro)}/SSA_{(total)}$ [%]
LC aerogel	106.5	100.2	6.2	94.1	5.8
Carbon aerogel	217.3	55.5	143.6	25.5	66.1

3.3.4 Hydrophobicity and Oil Spill Applications

LC is hydrophilic due to the hydroxyl groups present on the structures of lignin, cellulose, and hemicellulose. It was reported that a hydrophobic coating could be applied on a recycled

cellulose aerogel to make it oleophilic [21]. One of the main incentives to convert cellulose aerogels to be hydrophobic is because hydrophobic aerogels can repel water and attract oil, making them promising for applications such as oil spill cleaning [33]. Figure 20 shows the water contact angle (WCA) of 132.5 ° and 130.5 ° on an external and a freshly cut surface of the coated LC aerogel, respectively. This result suggests that the hydrophobic modification can reach deep into the LC aerogel, and the entire 3-D porous structure was converted to be hydrophobic.

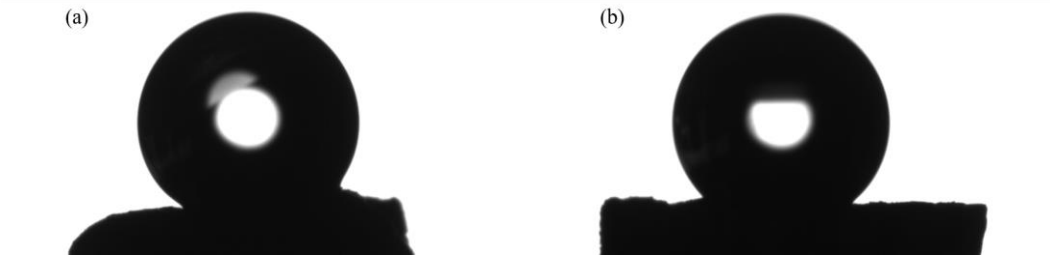

Figure 20. Water contact angle of the MTMS treated LC aerogel: (a) on an external surface, and (b) on a freshly cut surface.

In order to investigate the potential oil absorption performance of the surface-modified LC aerogel, pump oil, which was stained by Sudan III dye to show a higher visibility, was adopted for the demonstration, and the results are briefly presented in Figure 21. The surface modified LC aerogel can easily absorb the pump oil. At the beginning of the test, the stained pump oil was floating on water surface. Upon direct contact with the aerogel, the oil was quickly absorbed. After the completion of the absorption, the oil was completely removed and no stained oil was visibly detected on the water face. These results suggest that the modified LC aerogel could effectively absorb oil from water surface, offering an environmentally-friendly alternative option for oil spill cleaning.

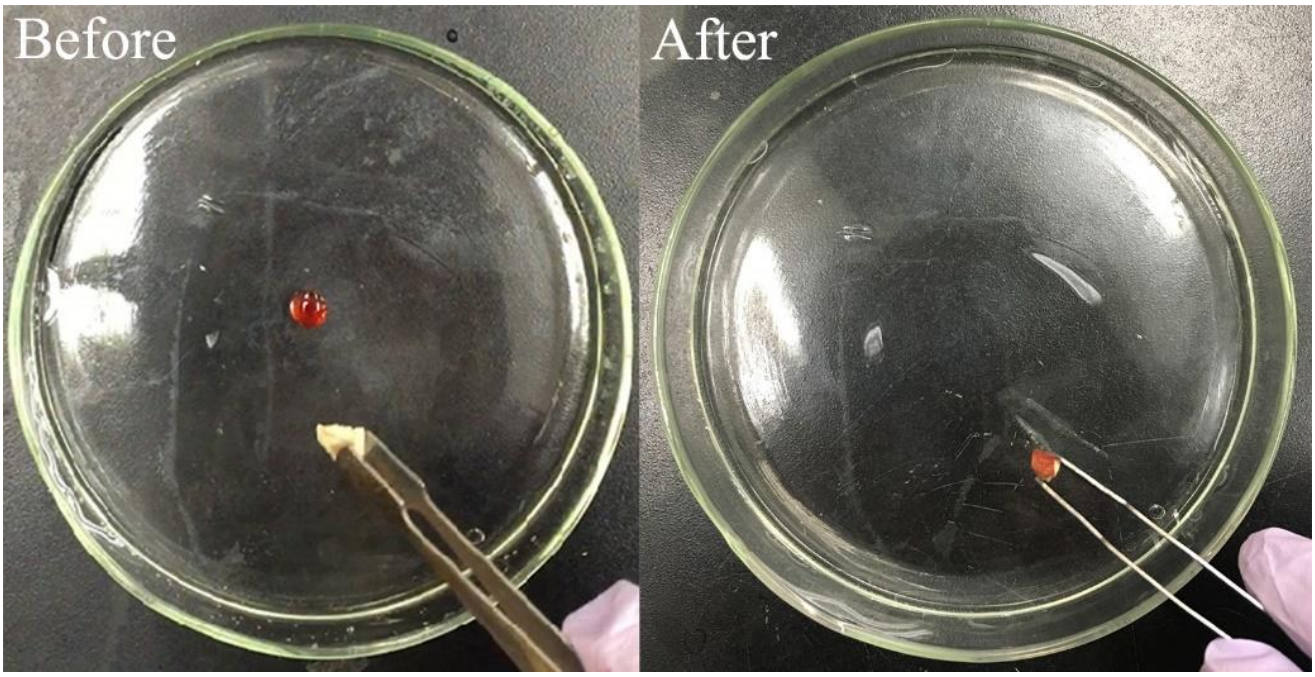

Figure 21. Pump oil absorption process by treated LC aerogel.

3.3.5 Silica nanoparticles from IL-RH residue

IL-RH residue was rinsed by DI water and dried in an oven. After it was dried, the residue was calcined at 700 ℃ for 2 hours. The XRD patterns shown in Figure 22 indicate that the silica derived from IL-RH residue remained to be amorphous. It exhibits a similar XRD pattern as the silica derived from HCl treated RHs (RH-HCl-silica) [9]. However, using the IL-RH residue to make silica contributes to the RH biomass comprehensive application strategy, which will improve the utilization efficiency of RHs and broaden the application of RH biomass [9].

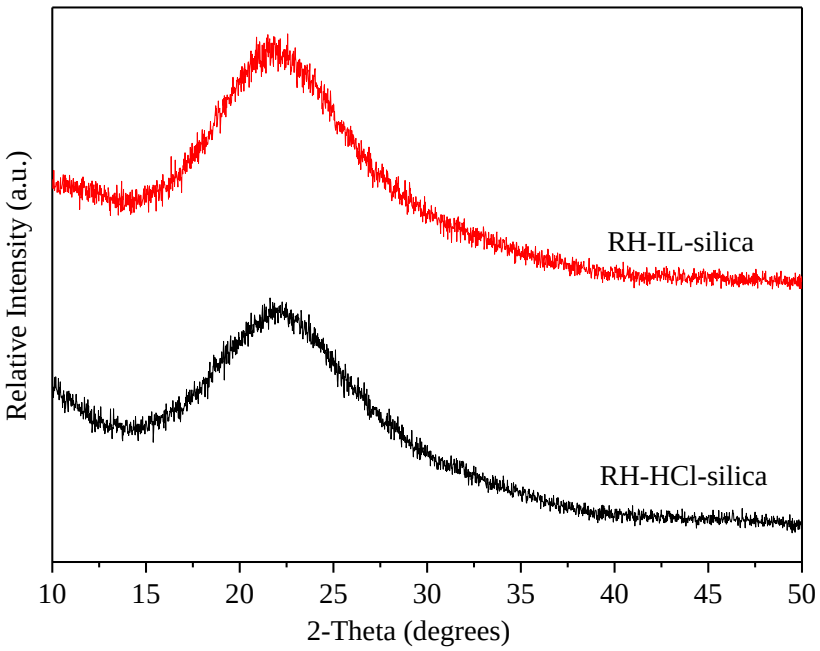

Figure 22. XRD patterns of the silica samples derived from IL-RH and HCl treated raw RHs.

3.4 Conclusion

In summary, the LC in RHs could be successfully dissolved into IL (BMIMCl) to form a homogenous solution. LC aerogel with a 3-D porous network structure was prepared by treating the LC IL solution with the NFT process. After the MTMS treatment, the LC aerogel turned from hydrophilic to hydrophobic. Such modified LC aerogel could potentially find applications in oil spill cleaning. The LC aerogel can be easily converted to carbon aerogel with a high surface area through a facile pyrolysis process. Meanwhile, silica nanoparticles could be prepared from the LC residue, leading to a comprehensive application of RHs.

References

1. Wang, Z.; Yu, J.; Zhang, X.; Li, N.; Liu, B.; Li, Y.; Wang, Y.; Wang, W.; Li, Y.; Zhang, L.; Dissanayake, S.; Suib, S. L.; Sun, L., Large-Scale and Controllable Synthesis of Graphene Quantum Dots from Rice Husk Biomass: A Comprehensive Utilization Strategy. *ACS Applied Materials & Interfaces* **2016,** *8* (2), 1434-1439.
2. Krishnarao, R.; Godkhindi, M., Distribution of silica in rice husks and its effect on the formation of silicon carbide. *Ceramics international* **1992,** *18* (4), 243-249.
3. Rahman, I.; Riley, F., The control of morphology in silicon nitride powder prepared from rice husk. *Journal of the European Ceramic Society* **1989,** *5* (1), 11-22.
4. Seo, E.; Andreoli, M.; Chiba, R., Silicon tetrachloride production by chlorination method using rice husk as raw material. *Journal of materials processing technology* **2003,** *141* (3), 351-356.
5. Wang, W.; Martin, J. C.; Huang, R.; Huang, W.; Liu, A.; Han, A.; Sun, L., Synthesis of silicon complexes from rice husk derived silica nanoparticles. *RSC Advances* **2012,** *2* (24), 9036-9041.
6. Sun, L.; Gong, K., Silicon-based materials from rice husks and their applications. *Industrial & engineering chemistry research* **2001,** *40* (25), 5861-5877.
7. Wang, Z.; Chen, H.; Xu, L.; Xu, S. Q.; Gao, C. F.; Oliphant, A. J.; Liu, J.; Lu, Y.; Wang, W.; Sun, L., Synthesis and colour prediction of stable pigments from rice husk biomass. *Green Materials* **2015,** *3* (1), 10-14.
8. Li, Y.; Lan, J. Y.; Liu, J.; Yu, J.; Luo, Z.; Wang, W.; Sun, L., Synthesis of Gold Nanoparticles on Rice Husk Silica for Catalysis Applications. *Industrial & engineering chemistry research* **2015,** *54* (21), 5656-5663.
9. Chen, H.; Wang, W.; Martin, J. C.; Oliphant, A. J.; Doerr, P. A.; Xu, J. F.; DeBorn, K. M.; Chen, C.; Sun, L., Extraction of lignocellulose and synthesis of porous silica nanoparticles from rice husks: a comprehensive utilization of rice husk biomass. *ACS Sustainable Chemistry & Engineering* **2012,** *1* (2), 254-259.
10. Saha, B. C. In *Lignocellulose biodegradation and applications in biotechnology*, ACS symposium series, Washington, DC; American Chemical Society; 1999: 2004; pp 2-35.
11. Yang, Q.; Fukuzumi, H.; Saito, T.; Isogai, A.; Zhang, L., Transparent cellulose films with high gas barrier properties fabricated from aqueous alkali/urea solutions. *Biomacromolecules* **2011,** *12* (7), 2766-2771.
12. Poplin, J. H.; Swatloski, R. P.; Holbrey, J. D.; Spear, S. K.; Metlen, A.; Grätzel, M.; Nazeeruddin, M. K.; Rogers, R. D., Sensor technologies based on a cellulose supported platform. *Chemical communications* **2007,** (20), 2025-2027.
13. Cai, J.; Kimura, S.; Wada, M.; Kuga, S.; Zhang, L., Cellulose aerogels from aqueous alkali hydroxide–urea solution. *ChemSusChem* **2008,** *1* (1-2), 149-154.
14. Ludueña, L.; Fasce, D.; Alvarez, V. A.; Stefani, P. M., Nanocellulose from rice husk following alkaline treatment to remove silica. *BioResources* **2011,** *6* (2), 1440-1453.
15. (a) Lee, S. H.; Doherty, T. V.; Linhardt, R. J.; Dordick, J. S., Ionic liquid-mediated selective extraction of lignin from wood leading to enhanced enzymatic cellulose hydrolysis. *Biotechnology and Bioengineering* **2009,** *102* (5), 1368-1376; (b) Zhu, S.; Wu, Y.; Chen, Q.; Yu, Z.; Wang, C.; Jin, S.; Ding, Y.; Wu, G., Dissolution of cellulose with ionic liquids and its application: a mini-review. *Green Chemistry* **2006,** *8* (4), 325-327.

16. Swatloski, R. P.; Spear, S. K.; Holbrey, J. D.; Rogers, R. D., Dissolution of cellose with ionic liquids. *Journal of the American Chemical Society* **2002,** *124* (18), 4974-4975.
17. Li, J.; Lu, Y.; Yang, D.; Sun, Q.; Liu, Y.; Zhao, H., Lignocellulose aerogel from wood-ionic liquid solution (1-allyl-3-methylimidazolium chloride) under freezing and thawing conditions. *Biomacromolecules* **2011,** *12* (5), 1860-1867.
18. Wu, Z.-S.; Yang, S.; Sun, Y.; Parvez, K.; Feng, X.; Müllen, K., 3D nitrogen-doped graphene aerogel-supported Fe3O4 nanoparticles as efficient electrocatalysts for the oxygen reduction reaction. *Journal of the American Chemical Society* **2012,** *134* (22), 9082-9085.
19. Aliev, A. E.; Oh, J.; Kozlov, M. E.; Kuznetsov, A. A.; Fang, S.; Fonseca, A. F.; Ovalle, R.; Lima, M. D.; Haque, M. H.; Gartstein, Y. N., Giant-stroke, superelastic carbon nanotube aerogel muscles. *science* **2009,** *323* (5921), 1575-1578.
20. Hu, Y.; Tong, X.; Zhuo, H.; Zhong, L.; Peng, X.; Wang, S.; Sun, R., 3D hierarchical porous N-doped carbon aerogel from renewable cellulose: an attractive carbon for high-performance supercapacitor electrodes and CO 2 adsorption. *RSC Advances* **2016,** *6* (19), 15788-15795.
21. Nguyen, S. T.; Feng, J.; Le, N. T.; Le, A. T.; Hoang, N.; Tan, V. B.; Duong, H. M., Cellulose aerogel from paper waste for crude oil spill cleaning. *Industrial & engineering chemistry research* **2013,** *52* (51), 18386-18391.
22. (a) Bi, H.; Yin, Z.; Cao, X.; Xie, X.; Tan, C.; Huang, X.; Chen, B.; Chen, F.; Yang, Q.; Bu, X., Carbon fiber aerogel made from raw cotton: a novel, efficient and recyclable sorbent for oils and organic solvents. *Advanced Materials* **2013,** *25* (41), 5916-5921; (b) Wu, Z. Y.; Li, C.; Liang, H. W.; Chen, J. F.; Yu, S. H., Ultralight, flexible, and fire-resistant carbon nanofiber aerogels from bacterial cellulose. *Angewandte Chemie* **2013,** *125* (10), 2997-3001.
23. (a) Ding, B.; Cai, J.; Huang, J.; Zhang, L.; Chen, Y.; Shi, X.; Du, Y.; Kuga, S., Facile preparation of robust and biocompatible chitin aerogels. *Journal of Materials Chemistry* **2012,** *22* (12), 5801-5809; (b) Lu, Y.; Sun, Q.; Yang, D.; She, X.; Yao, X.; Zhu, G.; Liu, Y.; Zhao, H.; Li, J., Fabrication of mesoporous lignocellulose aerogels from wood via cyclic liquid nitrogen freezing–thawing in ionic liquid solution. *Journal of Materials Chemistry* **2012,** *22* (27), 13548-13557.
24. (a) Li, J.; Wang, X.; Huang, Q.; Gamboa, S.; Sebastian, P., Studies on preparation and performances of carbon aerogel electrodes for the application of supercapacitor. *Journal of Power Sources* **2006,** *158* (1), 784-788; (b) Miller, J.; Dunn, B.; Tran, T.; Pekala, R., Deposition of ruthenium nanoparticles on carbon aerogels for high energy density supercapacitor electrodes. *Journal of the Electrochemical Society* **1997,** *144* (12), L309-L311; (c) Chien, H. C.; Cheng, W. Y.; Wang, Y. H.; Lu, S. Y., Ultrahigh specific capacitances for supercapacitors achieved by nickel cobaltite/carbon aerogel composites. *Advanced Functional Materials* **2012,** *22* (23), 5038-5043.
25. (a) Moreno-Castilla, C.; Maldonado-Hódar, F., Carbon aerogels for catalysis applications: An overview. *Carbon* **2005,** *43* (3), 455-465; (b) Biener, J.; Stadermann, M.; Suss, M.; Worsley, M. A.; Biener, M. M.; Rose, K. A.; Baumann, T. F., Advanced carbon aerogels for energy applications. *Energy & Environmental Science* **2011,** *4* (3), 656-667.
26. de Carvalho Mendes, C. A.; Ferreira, N. M. S.; Furtado, C. R. G.; de Sousa, A. M. F., Isolation and characterization of nanocrystalline cellulose from corn husk. *Materials Letters* **2015,** *148*, 26-29.
27. Xu, X.; Zhou, J.; Nagaraju, D. H.; Jiang, L.; Marinov, V. R.; Lubineau, G.; Alshareef, H. N.; Oh, M., Flexible, Highly Graphitized Carbon Aerogels Based on Bacterial Cellulose/Lignin: Catalyst-Free Synthesis and its Application in Energy Storage Devices. *Advanced Functional Materials* **2015,** *25* (21), 3193-3202.

28. Kalita, E.; Nath, B.; Deb, P.; Agan, F.; Islam, M. R.; Saikia, K., High quality fluorescent cellulose nanofibers from endemic rice husk: Isolation and characterization. *Carbohydrate polymers* **2015,** *122*, 308-313.
29. Sun, X.; Chi, Y.; Mu, T., Studies on staged precipitation of cellulose from an ionic liquid by compressed carbon dioxide. *Green Chemistry* **2014,** *16* (5), 2736-2744.
30. (a) Tang, S.; Baker, G. A.; Ravula, S.; Jones, J. E.; Zhao, H., PEG-functionalized ionic liquids for cellulose dissolution and saccharification. *Green Chemistry* **2012,** *14* (10), 2922-2932; (b) Cheng, G.; Varanasi, P.; Li, C.; Liu, H.; Melnichenko, Y. B.; Simmons, B. A.; Kent, M. S.; Singh, S., Transition of cellulose crystalline structure and surface morphology of biomass as a function of ionic liquid pretreatment and its relation to enzymatic hydrolysis. *Biomacromolecules* **2011,** *12* (4), 933-941.
31. Li, W.; Sun, N.; Stoner, B.; Jiang, X.; Lu, X.; Rogers, R. D., Rapid dissolution of lignocellulosic biomass in ionic liquids using temperatures above the glass transition of lignin. *Green Chemistry* **2011,** *13* (8), 2038-2047.
32. Gani, A.; Naruse, I., Effect of cellulose and lignin content on pyrolysis and combustion characteristics for several types of biomass. *Renewable Energy* **2007,** *32* (4), 649-661.
33. Xiao, S.; Gao, R.; Lu, Y.; Li, J.; Sun, Q., Fabrication and characterization of nanofibrillated cellulose and its aerogels from natural pine needles. *Carbohydrate polymers* **2015,** *119*, 202-209.

Chapter 4. Summary and Outlook

4.1 Summary

Rice Husks (RHs) are one of the most available and abundant biomasses in the world, and could be consider as a "true" biomass as they are the byproduct after rice milling. They have been applied in many different fields including chemistry, biology, materials science, and environmental protection. However, during most conventional utilizations of RHs, researchers focus on one component of RHs (such as silica) while ignore others. Achieve a comprehensive utilization of RHs and generating product diversity should be the goal for the future research in this field. In this thesis, two main components of RH biomass were extracted: silica and lignocellulose. A calcination method was adopted to prepare silica from RHs. The synthesized silica nanoparticles could be used for the synthesis of green phosphor $Zn_2SiO_4:Mn^{2+}$ because of its high reactivity. This study also experimented with and discussed the effects of reaction temperature and doping concentration of Mn^{2+} on the photoluminescence performance of the synthesized phosphors. Compared with the phosphors synthesized from commercial silica, this plant-sourced phosphor is a promising alternative because of its low price and better photoluminescence properties. For the second part of this study, lignocellulose was extracted by using ionic liquid (BMIMCL). Highly light and porous lignocellulose aerogel was synthesized via a freeze-thaw process, water regeneration, and CO_2 supercritical drying. After surface modification, the lignocellulose aerogel exhibited highly hydrophobic property, making it effective in oil spill adsorption. In addition, carbon aerogel was prepared when the lignocellulose aerogel was pyrolyzed at high temperatures under an inert gas atmosphere, which can potentially be used for supercapacitors. Following the comprehensive application strategy, the RH residue was utilized to prepare high purity amorphous silica, which can be used to make various silica derived chemicals,

such as silicate phosphors. This project explored the comprehensive utilization of RH biomass by producing two major products for various applications.

4.2 Outlook

While this project and most current research in this field focus on deriving various valuable products from RHs for practical applications, how to better tailor the morphology of the basic products should be another major focus for future research. Although amorphous silica nanoparticles with a high surface area has been synthesized from RHs, they form clusters and thus not well separated with each other, thus cannot be well dispersed to form a stable dispersion. This defect is the major barrier that limits RH-silica for many more advanced applications, such as silica based core-shell structured catalysts and biomedical applications. For the lignocellulose from RHs, many new applications can be explored if the morphology of the lignocellulose can be better tailored. For example, cellulose nanocrystals can possibly be derived from RHs, which have promising applications in composites.